

Spitzer's perspective of polycyclic aromatic hydrocarbons in galaxies

Aigen Li

Department of Physics and Astronomy, University of Missouri, Columbia, MO 65211, USA. e-mail: lia@missouri.edu

Polycyclic aromatic hydrocarbon (PAH) molecules, as revealed by the distinctive set of emission bands at 3.3, 6.2, 7.7, 8.6, 11.3 and 12.7 μm characteristic of their vibrational modes, are abundant and widespread throughout the Universe. They are ubiquitously seen in a wide variety of astrophysical regions, ranging from planet-forming disks around young stars to the interstellar medium (ISM) of the Milky Way and external galaxies out to high redshifts at $z \gtrsim 4$. PAHs profoundly influence the thermal budget and chemistry of the ISM by dominating the photoelectric heating of the gas and controlling the ionization balance. Here, we review the current state of knowledge of the astrophysics of PAHs, focusing on their observational characteristics obtained from the *Spitzer Space Telescope* and their diagnostic power for probing the local physical and chemical conditions and processes. Special attention is paid to the spectral properties of PAHs and their variations revealed by the *Infrared Spectrograph (IRS)* on board *Spitzer* across a much broader range of extragalactic environments (e.g., distant galaxies, early-type galaxies, galactic halos, active galactic nuclei, and low-metallicity galaxies) than was previously possible with the *Infrared Space Observatory (ISO)* or any other telescope facilities. Also highlighted is the relation between the PAH abundance and the galaxy metallicity established for the first time by *Spitzer*.

In the early 1970s, a new chapter in astrochemistry was opened first by Gillett et al.¹ who, based on ground observations, detected three prominent emission bands peaking at 8.6, 11.3 and 12.7 μm in the 8–14 μm spectra of two planetary nebulae, NGC 7027 and BD + 30°3639. Two years later, Merrill et al.² reported the detection of a broad emission band at 3.3 μm , again in NGC 7027. Also around that time, airborne observations became possible. This led to the detection of two additional, ground-inaccessible intense emission bands at 6.2 and 7.7 μm in NGC 7027 (ref.³) and M82, an external galaxy⁴, with the *Kuiper Airborne Observatory (KAO)*. Subsequently, all these features at 3.3, 6.2, 7.7, 8.6, 11.3, and 12.7 μm were found to be widespread throughout the Universe and closely related to form a family, exhibiting an overall similar spectral profile among different sources (see Fig. 1).

Although the exact nature of their carriers remains unknown — because of this, they are collectively known as the “unidentified” IR emission (UIE) features — the hypothesis of PAH molecules as the carriers^{5,6} has gained widespread acceptance and extreme popularity. The PAH model attributes the UIE bands to the vibrational modes of PAHs composed of fused benzene rings of several tens to several hundreds of C atoms, with the 3.3 μm band assigned to C–H stretching modes, the 6.2 μm and 7.7 μm bands to C–C stretching modes, the 8.6 μm band to C–H in-plane bending modes, and the 11.3 and 12.7 μm bands to C–H out-of-plane (CH_{oop}) bending modes. The relative strengths of these bands depend not only on the size, structure, and charging of the PAH molecule, but also on the local physical conditions^{7–10}.

It is now well recognized that PAHs are an essential component of the interstellar medium (ISM) and play an important role in many aspects of astrophysics. They account for

$\lesssim 15\%$ of the interstellar carbon^{9–13} and their emission accounts for up to 20% of the total IR power of the Milky Way and star-forming galaxies^{14,15}. Therefore by implication, they must be an important absorber of starlight^{16–18} and are possibly related to or even responsible for some of the longstanding unexplained interstellar phenomena (e.g., the 2175 Å extinction bump^{9,16,19}, the diffuse interstellar bands²⁰, the blue and extended red photoluminescence emission²¹, and the “anomalous microwave emission”^{22,23}). PAHs profoundly influence the thermal budget and chemistry of the ISM. They dominate the heating of the gas in the diffuse ISM as well as the surface layers of protoplanetary disks by providing photoelectrons^{24–26}. As an important sink for electrons, PAHs dominate the ionization balance in molecular clouds and hence they influence the ion-molecule chemistry and the ambipolar diffusion process that sets the stage for star formation²⁷.

In this review, we provide an overview of the current state of knowledge of the astrophysics of PAHs, with details on their observational characteristics obtained from the *Spitzer Space Telescope*. Special attention is also paid to their diagnostic capabilities to probe the local physical and chemical conditions as well as their reactions to different environments. We focus on *Spitzer* results, but the science case often builds on pioneering observations performed prior to *Spitzer* with ground-based, airborne and space telescopes, in particular the *Infrared Space Observatory (ISO)*. We discuss the properties of PAHs in the context of both *Spitzer* observations and observations obtained with prior and other contemporary telescope facilities.

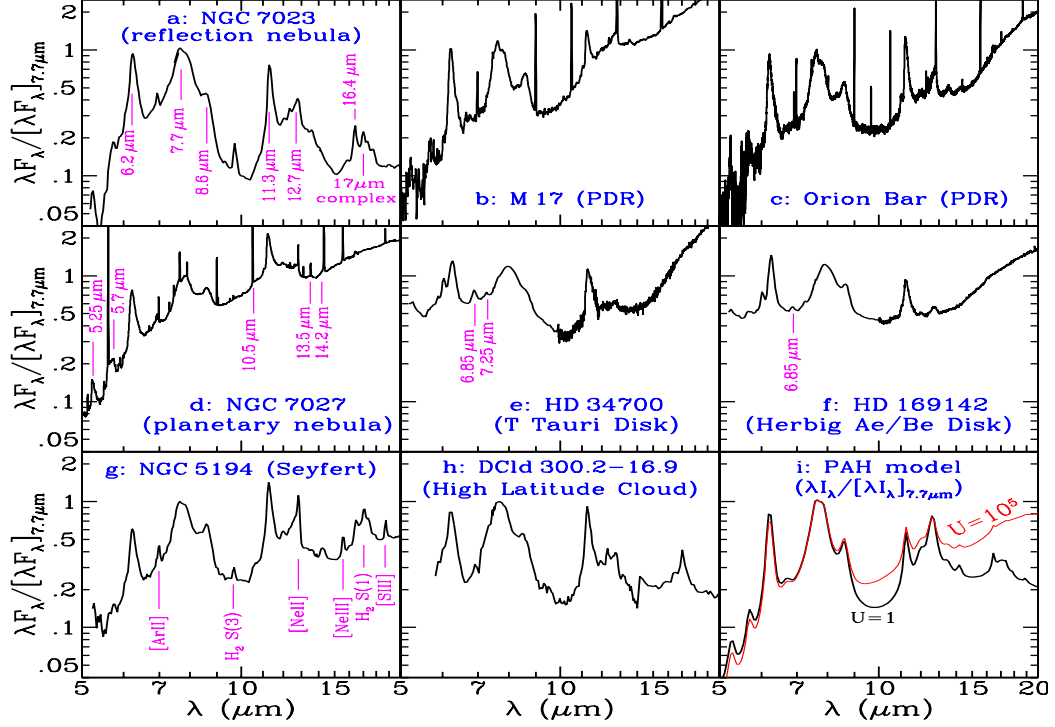


Figure 1: **Observed and model-predicted 5–20 μm PAH spectra.** (a) Reflection nebula NGC 7023 (ref.⁵⁷); (b) M17 PDR¹⁷²; (c) Orion Bar PDR¹⁷³; (d) Planetary nebula NGC 7027 (ref.¹⁷⁴); (e) T Tauri disk HD 34700 (ref.¹⁷⁵); (f) Herbig Ae/Be disk HD 169142 (ref.¹⁷⁶); (g) Seyfert grand-design spiral galaxy NGC 5194 (ref.¹⁴); (h) Translucent high Galactic latitude cloud DCld 300.2-16.9 (ref.⁵⁰); (i) Model emission calculated for PAHs illuminated by the local interstellar radiation field¹⁷⁷ (i.e., $U = 1$; black line) or a much more intense radiation field (i.e., $U = 10^5$; red line)¹⁰. The major PAH bands are labelled in (a). Some of the weak, secondary PAH bands (superimposed by sharp gas lines) are labelled in (d). The 6.85 and 7.25 μm aliphatic C–H deformation bands are labelled in (e) and (f) for protoplanetary disks. The sharp gaseous emission lines are labelled in (g)^{178,179}.

PAHs in the pre-*Spitzer* era

Over the intervening 30 years between the first detection of PAHs in 1973 (ref.¹) and the launch of *Spitzer* in 2003, numerous ground-based, airborne and spaceborne observations have substantially promoted or even revolutionized our understanding of PAHs in astrophysics. These observations have established that PAHs are an ubiquitous and abundant component of a wide variety of astrophysical regions, ranging from planetary nebulae, protoplanetary nebulae, reflection nebulae, HII regions, the Galactic IR cirrus, and protoplanetary disks around Herbig Ae/Be stars to the ISM of both normal and active nearby galaxies^{15,28}. Most notably, Sellgren et al.²⁹ showed that in three reflection nebulae (NGC 7023, NGC 2023, and NGC 2068) the 3.3 μm feature profile shows very little variation with distance from the central star, revealing the emission mechanism of the PAH bands as due to the IR fluorescence from molecule-sized species vibrationally excited by individual UV/visible photons^{7,30,31}.

Thanks in large part to the fact that the 3 μm region and the 8–14 μm region are accessible to ground-based telescopes, in the 1980s and 1990s the C–H stretching bands at 3.3 μm and the CH_{oop} bending bands at 11.3 μm were the subject of extensive scrutiny. Careful observations revealed a great deal about the detailed spectral and spatial structures of the emission bands in

these regions. The C–H stretch near 3 μm exhibits a rich spectrum: the dominant 3.3 μm feature is usually accompanied by a weaker feature at 3.4 μm along with an underlying plateau extending out to $\sim 3.6 \mu\text{m}$. In some objects, a series of weaker features at 3.46, 3.51, and 3.56 μm are also seen superimposed on the plateau, showing a tendency to decrease in strength with increasing wavelength^{32–34}. Similarly, the 11.3 μm band is also generally accompanied by a second distinct, but weaker, feature near 12.7 μm . Weaker features are also often present near 11.0, 11.5, 12.0, and 13.5 μm (ref.³⁵), arising from the CH_{oop} bending vibrations of PAHs.

In the 1970s and 1980s, the 6.2 and 7.7 μm bands were only accessible from KAO. KAO observations had already revealed significant variations in the PAH feature profiles among different types of sources. Typically, harsh environments like planetary nebulae, reflection nebulae and HII regions, in which the dust has been heavily processed, show “normal”-looking PAH spectra. The 7.7 and 8.6 μm bands of these sources are well-separated. In contrast, some benign protoplanetary nebulae, in which the dust is relatively fresh, exhibit a broad 8 μm complex³⁶. The CH_{oop} bending bands of those heavily processed sources also differ from that of less processed sources: while the former exhibit a prominent 11.3 μm band and a weaker but distinct 12.7 μm band, the latter intend to only show a broad complex at $\sim 12 \mu\text{m}$. In ad-

dition, those less processed sources often have a much stronger 3.4 μm band (which is often comparable to or even stronger than the 3.3 μm band). Finally, KAO observations had also showed that the 7.7 μm band may be comprised of at least two variable components³⁷.

ISO provided the first opportunity to obtain complete IR spectra from 2.4–197 μm unobscured by telluric absorption. Spanning a wavelength range of 2.4 to 45 μm , the *Short Wavelength Spectrometer* (SWS) on board ISO was well suited to surveying the PAH emission and obtaining a census of the PAH bands³⁸. A new PAH band at 16.4 μm was discovered in the ISO/SWS spectra of various sources³⁹. Also, the aromatic C–H and C–C bands at 3.3 and 6.2 μm were seen in *absorption* in the ISO/SWS spectra of heavily obscured local sources as well as sources toward the Galactic center^{40,41}. The superb spectral resolving power of ISO/SWS found that many of the prominent bands show satellite bands or break up into subfeatures³⁸. Moreover, the ISO/SWS observations have revealed systematic variations in the profiles and relative intensities of the PAH bands from source to source and spatially within sources³⁸. Based primarily on the variations of the 7.7 μm band seen in the ISO/SWS spectra, Peeters et al.⁴² classified the PAH sources into three classes. Furthermore, the 5.8–11.6 μm ISOPHOT low-resolution spectrophotometer PHT-S on board ISO for the first time detected the 6.2, 7.7, 8.6 and 11.3 μm PAH bands in the diffuse emission of the Galactic disk⁴³. Although the starlight intensity in the Galactic disk is substantially lower than that of typical reflection nebulae and planetary nebulae by a factor of ~ 100 –1000, the profiles and relative intensities of the PAH bands are closely similar to the “normal”-looking PAH spectra of reflection nebulae and planetary nebulae (see Fig. 2d). At about the same time, the advent of the Japanese *Infrared Telescope in Space* (IRTS) also detected the 3.3–11.3 μm PAH bands in the diffuse emission near the Galactic plane^{44,45}.

The *Spitzer* legacy of PAH astrophysics

Owing to its up to a factor of 100 better sensitivity than ISO/SWS, *Spitzer* allowed one to extend the mid-IR spectroscopy and imaging into new regimes that ISO could not probe. The *Infrared Spectrograph* (IRS) on board *Spitzer* was capable of detecting PAH emission in objects which were too faint for ISO (e.g., the PAH emission at 6–9 μm of protoplanetary disks around T Tauri stars which had previously escaped detection by ISO⁴⁶ was unambiguously detected by *Spitzer*/IRS^{47–49}; see Fig. 1e). *Spitzer* was able to probe PAHs in much larger samples spanning much wider varieties of astrophysical environments, from low-UV translucent high Galactic latitude clouds⁵⁰ to UV-intense regions. Therefore, the systematic trends and characteristics of PAHs as well as the exploitation of the PAH bands as diagnostics of the physical and chemical conditions and processes could be determined in an unbiased manner. Also, the high sensitivity of *Spitzer*/IRS enabled unprecedented PAH spectral mapping of both Galactic and extragalactic sources^{51–55}. Complemented with observations by, e.g., ISO and the Japanese AKARI infrared satellite, *Spitzer* made lasting contributions and substantially expanded our knowledge about the physical and chemical properties of PAHs and their important role in astrophysics.

The *Spitzer* inventory of PAH spectra. Compared with ISO/SWS, the main limitations of *Spitzer*/IRS were its relatively lower spectral resolution and narrower wavelength coverage. The spectral resolution of *Spitzer*/IRS in the 5–10 μm wavelength range was lower than that of ISO/SWS by more than an order of magnitude. Also, operating at 5–38 μm , *Spitzer*/IRS unfortunately missed the PAH C–H stretch at 3.3 μm . Nevertheless, despite its limited spectroscopic capabilities, *Spitzer*/IRS pioneered both in discovering new PAH bands and in showcasing the richness and complexity of the PAH spectra, particularly at wavelengths longward of ~ 10 μm . The *Spitzer*/IRS spectroscopy of the star-forming ring in the spiral galaxy NGC 7331 unambiguously revealed, for the first time, a strong, broad emission feature centered at 17.1 μm , with a width of ~ 0.96 μm and an intensity three times as strong as the 16.4 μm feature or nearly half as strong as the ubiquitous 11.3 μm band⁵⁶. As illustrated in Fig. 1a and 1g, this prominent feature is widely seen in the *Spitzer*/IRS spectra of both Galactic and extragalactic sources^{14,57}. The presence of this feature had been hinted by the ISO/SWS spectra of Galactic sources^{7,58}. In addition, Werner et al.⁵⁷ reported discovery of new PAH features at 15.8 and 17.4 μm in the *Spitzer*/IRS spectra of NGC 7023, together with a new feature at 18.9 μm whose carrier was later identified as C₆₀^{60,61}. The 16.4, 17.1, and 17.4 μm PAH features, resulting from in-plane and out-of-plane ring bending modes of the carbon skeleton, constitute the so-called 17 μm complex. As the strongest PAH band longward of 12 μm , the 17 μm complex is dominated by the broad 17.1 μm band, with the distinct flanking subfeatures at 16.4 and 17.4 μm contributing only $\sim 20\%$ of the total power in the complex¹⁴.

Spitzer/IRS observations reinforced the richness of the PAH spectra. Together with ISO/SWS observations, *Spitzer*/IRS observations revealed that, apart from the major bands at 6.2, 7.7, 8.6, 11.3 and 12.7 μm which dominate the mid-IR emission spectra of many objects, there are also weaker, secondary features at 5.25, 5.7, 6.0, 6.7, 8.3, 10.5, 11.0, 12.0, 13.6, 14.2, 15.8, 16.4, 17.4 and 17.8 μm as well as underlying broad continuum emission plateaus^{14,15,38}. The CH_{oop} bending bands at wavelengths longward of ~ 10 μm are of particular interest. They are characteristic of the edge structure of PAHs and occur at different wavelengths, depending on the number of neighbouring hydrogen atoms on one aromatic ring: for neutral PAHs, isolated CH_{oop} band (solo-CH) occurs at ~ 11.3 μm , doubly adjacent CH (duet-CH) at ~ 12.0 μm , triply adjacent CH (trio-CH) at ~ 12.7 μm , and quadruply adjacent CH at ~ 13.6 μm (ref.^{62,63}). Hudgins & Allamandola⁶⁴ experimentally showed that the aromatic CH_{oop} bending wavelengths are significantly blue-shifted upon ionization.

In the 6–9 μm wavelength range, *Spitzer*/IRS observations found that the 7.7 μm band of some carbon-rich post-asymptotic giant branch (post-AGB) stars in the Large Magellanic Cloud (LMC)⁶⁵ and Small Magellanic Cloud (SMC)⁶⁶ exhibits more pronounced profile variations than previously revealed by ISO/SWS observations for Galactic sources. While the profile variations of the 7.7 μm band seen in the ISO/SWS spectra were employed as a spectral classification scheme⁴², the *Spitzer*/IRS observations led to further classifications of the PAH spectra^{65,66}. Moreover, the subtle variations in the peak wavelength of the 6.2 μm emission band, commonly attributed to polycyclic aromatic nitrogen heterocycles — PAHs with one or more

nitrogen atoms substituted into their carbon skeleton⁶⁷ — were recently seen in the *Spitzer*/IRS spectra of starburst galaxies⁶⁸.

2D spectral and photometric mapping of PAH emission with *Spitzer*. While ISOCAM, the camera on board ISO, had an imaging capability with its narrow-band filters which cover the major PAH bands, its observation was quite limited because of its sensitivity. Thanks to the much higher sensitivity of *Spitzer*/IRS, 2D spectral mapping observations of PAH emission became possible. *Spitzer*/IRS provided for the first time significant data that allow us to study the spatial distribution of PAH emission and quantitatively investigate the spatial variations of the PAH size, structure, and ionization and their responses to changing environments^{53–55}. Berné et al.⁶⁹ applied the so-called *Blind Component Separation* method to analyze the *Spitzer*/IRS 2D spectral mapping data of several Galactic objects. They showed that the observed PAH emission can be decomposed into three components, respectively arising from neutral PAHs, ionized PAHs, and PAH clusters or very small grains. The spatial distributions of these components provide useful information on their photochemical evolution and the local physical conditions. The viability of this method depends on how applicable the adopted template emission spectra of neutral PAHs, ionized PAHs, and PAH clusters are to various astrophysical regions whose PAH emission spectra are diverse.

The 8 μm broadband imaging photometer of the *Infrared Array Camera* (IRAC) on board *Spitzer* also provided a unique opportunity to explore the spatial distribution of PAHs both in extended Galactic sources and in spatially resolved external galaxies, as the IRAC 8 μm emission is dominated by the 6.2, 7.7 and 8.6 μm bands of PAHs. The 8 μm *Spitzer*/IRAC mapping of the M17 HII region clearly revealed the paucity of PAH emission in HII regions, indicating the destruction of PAHs by extreme UV photons within HII regions⁷⁰.

PAHs in the early Universe. Although distant galaxies are too faint to be subject to direct ISO/SWS spectroscopy, Elbaz et al.⁷¹ found that the rest-frame 5–25 μm spectral energy distributions (SEDs) of a sample of 16 distant luminous infrared galaxies (LIRGs) at redshifts $z \sim 0.1$ –1.2, constructed from the 15 μm photometry of ISOCAM and the 24 μm photometry of the *Multi-band Imaging Photometer* (MIPS) on board *Spitzer*, indicated the presence of the 7.7 μm PAH band in more than half of the sample. However, as illustrated in Fig. 2, *Spitzer* provided the first spectroscopic evidence for the presence of PAHs in distant galaxies. Yan et al.⁷² reported clear detection of multiple PAH emission bands in the *Spitzer*/IRS spectra of ultraluminous infrared galaxies (ULIRGs) at $z \sim 2$. Lutz et al.⁷³ also detected the PAH emission bands in the *Spitzer*/IRS spectra of two luminous submillimeter galaxies at $z \sim 2.8$. Also, the 6.2 and 7.7 μm bands of PAHs were clearly seen in the *Spitzer*/IRS spectrum of the Cosmic Eye, a strongly lensed, star-forming Lyman break galaxy at $z = 3.074$ (ref.⁷⁴). As shown in Fig. 2, the PAH spectra of both the Cosmic Eye and the submm galaxies of Lutz et al.⁷³ are “normal”-looking, exhibiting close similarity to that of the Galactic diffuse ISM⁴³. More recently, the 6.2 μm PAH band was detected in the *Spitzer*/IRS spectrum of the $z = 4.055$ submillimeter galaxy GN20, one of the intrinsically brightest submillimeter galaxies known⁷⁵, indicating that complex aromatic organic molecules were already prevalent in the young universe, only ~ 1.5 Gyr after the Big Bang. As PAHs play an important role in prebiotic chemistry which may ultimately lead to the de-

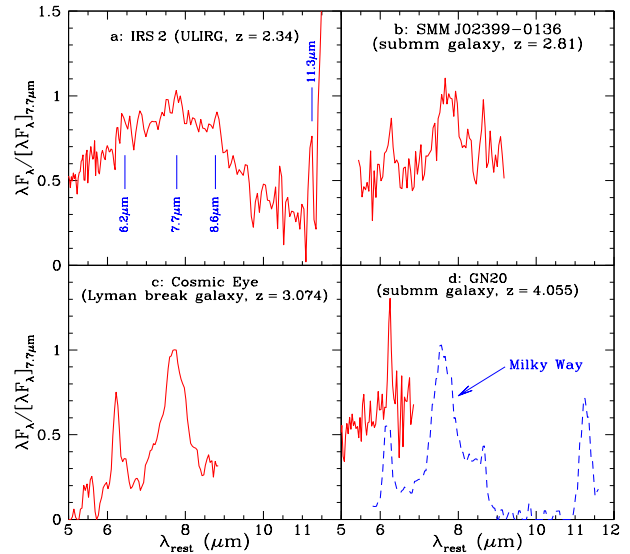


Figure 2: *Spitzer*/IRS rest-frame spectra of galaxies at high redshifts. (a) ULIRG IRS 2 ($z = 2.34$)⁷²; (b) Submm galaxy SMM J02399-0136 ($z = 2.81$)⁷³; (c) Lyman break galaxy Cosmic Eye ($z = 3.074$)⁷⁴; and (d) Submm galaxy GN20 ($z = 4.055$)⁷⁵. Also shown in (d) is the ISOPHOT spectrum of the Galactic diffuse ISM (blue dashed line)⁴³.

velopment of organic life, the detection of PAHs in the early Universe has important astrophysical implications^{76,77}.

Because the PAH features are so prevalent and intense in distant galaxies as indicated by *Spitzer*/IRS observations, in the future eras of the *James Webb Space Telescope* (JWST) and the *Space Infrared Telescope for Cosmology and Astrophysics* (SPICA), they might be used as redshift indicators. The integrated luminosity from the PAH features at 6.2, 7.7, and 11.3 μm has been shown to correlate linearly with the star formation rate (SFR) as measured by the extinction-corrected H α luminosity for 105 galaxies of IR luminosities $\sim 10^9$ – $10^{12} L_{\odot}$ at $0 < z < 0.4$ (ref.⁷⁸). The luminosity of the individual 6.2, 7.7 and 11.3 μm PAH bands has also been shown to correlate well with the IR luminosity for both local starburst galaxies and high-redshift submm galaxies including GN20 (ref.^{75,79}). These suggest that PAH emission could also be used as an accurate, quantitative measure of the SFR (but also see ref.^{80,81}) across cosmic time up to high redshifts to study the star formation history of the Universe. While the *Mid-Infrared Instrument* (MIRI) on board JWST which covers the wavelength range of 5 to 28 μm will limit the detection of the 6.2 μm PAH band to $z \lesssim 3$, the SPICA *Far Infrared Instrument* (SAFARI), operating at 35–230 μm , will enable the detection of PAHs in the very first galaxies in the Universe⁸².

PAHs in early-type galaxies. For a long time, early-type galaxies (i.e., E and S0 galaxies) were thought to be essentially devoid of interstellar matter. The detection of PAHs in elliptical galaxies with *Spitzer*/IRS for the first time by Kaneda et al.^{83,84} demonstrated that, adding to the earlier detection of hot gas and cold dust, elliptical galaxies contain a considerable amount of interstellar matter. Vega et al.⁸⁵ also reported the detection of PAH

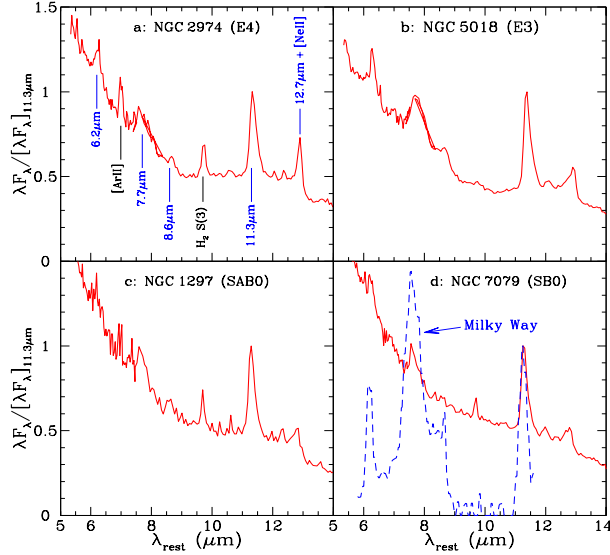


Figure 3: *Spitzer*/IRS spectra of early-type galaxies. (a) Elliptical galaxy NGC 2974 of type E4 in Hubble’s classification scheme⁸⁴; (b) E3 elliptical galaxy NGC 5018 (ref.⁸⁴); (c) SAB0 lenticular galaxy NGC 1297 (ref.⁸⁵); and (d) SB0 barred lenticular galaxy NGC 7079 (ref.⁸⁵). In (a) both the PAH bands and the gaseous lines are labelled, where the 12.7 μm band is blended with [NeII]. Also shown in (d) is the ISOPHOT spectrum of the Galactic diffuse ISM (blue dashed line)⁴³. Compared to the Galactic diffuse ISM of which the 6.2, 7.7 and 8.6 μm bands prevail, the PAH spectra of early-type galaxies are dominated by the 11.3 μm band.

emission in the *Spitzer*/IRS spectra of S0 galaxies. As illustrated in Fig. 3, the PAH spectra of early-type galaxies exhibit a strong enhancement at the 11.3 μm band and substantial suppression at the 7.7 μm band^{83–85}. The peculiar 11.3/7.7 band ratios seen in elliptical (and S0) galaxies indicate that the PAH size distribution is skewed toward appreciably larger molecules. In the hostile environments of elliptical galaxies (containing hot gas of temperature $\sim 10^7$ K), small PAHs can be easily destroyed through sputtering by plasma ions. This calls into question the origin of PAHs (and more generally, dust and gas) in ellipticals: are they from internal processes such as mass loss of red giants, or from mergers with spirals or small dust-rich irregular galaxies, or alternatively, could they be made in dense gas in a disk that has cooled out of the hot ISM? Kaneda et al.⁸⁴ found that the 11.3 μm PAH emission of elliptical galaxies correlates well with the dust continuum emission at 35 μm , whereas it does not correlate with the stellar photospheric emission at 6 μm . Therefore, they suggested that PAHs in elliptical galaxies are mostly of interstellar origin rather than of stellar origin. However, it is also possible that, as long as the quantities of PAHs and dust are both proportional to the amount of interstellar material in these elliptical galaxies, it does not matter where PAHs were formed and one expects the dust continuum emission to correlate with PAH emission. The lack of correlation between starlight and PAH emission could also be explainable if the excitation of PAHs in elliptical galaxies is dominated by electronic collisions instead of stellar photons. In any case, the detection of PAHs in early-type galaxies provide useful constraints on the evolution of the ISM in the harsh environments

of these galaxies.

PAHs in galaxy halos. Irwin & Madden⁸⁶ analyzed the ISO-CAM maps of NGC 5907, an edge-on galaxy with a low SFR of $\sim 1.2M_{\odot} \text{ yr}^{-1}$, in four narrow bands centering at 6.8, 7.7, 9.6, and 11.3 μm . They found that the IR emission seen in these bands extends as far as 6.5 kpc from the plane. As the ISOCAM narrow-band photometry at 6.8, 7.7, 9.6, and 11.3 μm traces PAH emission, they suggested that PAHs are present in the halo of NGC 5907.

Engelbracht et al.⁸⁷ obtained the *Spitzer*/IRAC images of the archetypal starburst, superwind galaxy M82 in which the central starburst drives a galactic outflow or superwind perpendicular to the galaxy plane. As shown in Fig. 4, the IRAC 8 μm emission, generally attributed to PAHs, extends at least 6 kpc from the plane and is seen all around the galaxy, well beyond the cone defined by the superwind. Engelbracht et al.⁸⁷ also obtained the *Spitzer*/IRS spectra for M82 and clearly detected the 16.4 and 17.1 μm bands of PAHs in its superwind region.

Beirão et al.⁸⁸ mapped the superwind/halo region of M82 with *Spitzer*/IRS and obtained spatially resolved PAH spectra. They found that the interband ratios of the 6.2, 7.7 and 11.3 μm features vary by more than a factor of five across the superwind region. As illustrated in Fig. 4, the intensities of the 11.3, 12.7 and 17.1 μm bands relative to the 6.2, 7.7 and 8.6 μm bands are stronger in both the north and south superwinds than in the center, suggesting that the PAH molecules in the superwind are somewhat larger, probably resulting from preferential destruction of smaller PAHs in the harsh superwind by X-rays and/or shocks.

With AKARI, Yamagishi et al.⁸⁹ obtained the spatially-resolved 2.5–4.5 μm near-IR spectra of M82 and detected the 3.3 μm PAH emission as well as the 3.4 μm emission complex both in the center and in the superwind, with the intensity ratio of the 3.4 μm complex to the 3.3 μm feature appreciably increasing with distance from the plane. As shown in Fig. 4, in the center the 3.4 μm feature is much weaker than the 3.3 μm feature, in contrast, in the superwind the 3.4 μm feature supercedes the 3.3 μm feature and dominates the near-IR spectra. While the 3.3 μm emission arises from the aromatic C–H stretch, the 3.4 μm complex is commonly attributed to the aliphatic side chains attached as functional groups to the aromatic skeleton of PAHs^{32–34}, although superhydrogenated PAHs (i.e., PAHs whose edges contain excess H atoms) of which the extra H atom converts the originally aromatic ring into an aliphatic ring^{90–94}, and the anharmonicity of the aromatic C–H stretch^{95,96} could also be responsible for the 3.4 μm feature. The intensity ratio of the 3.4 μm aliphatic band to the 3.3 μm aromatic band is often used to derive the aliphatic fraction (i.e., the fraction of carbon atoms in aliphatic form) of PAHs^{97–99}. It is puzzling that the PAH aliphatic fraction is considerably higher in the superwind than in the center. One would imagine that in the harsh superwind environment PAHs would be easily stripped off any aliphatic sidegroups. For PAHs with an appreciable aliphatic fraction, the 6.85 and 7.25 μm aliphatic C–H deformation bands¹⁰⁰ would show up (e.g., see Fig. 1e). However, a close inspection of Fig. 4 reveals no evidence for these two bands in the *Spitzer*/IRS spectra of M82, neither in the center nor in the superwind. It is also puzzling how small PAHs of ~ 20 –30 C atoms which emit at 3.3 μm ¹⁰ could survive in the superwind. Yamagishi et al.⁸⁹ suggested that they are produced *in situ* by shattering of large grains. Alternatively, they may be

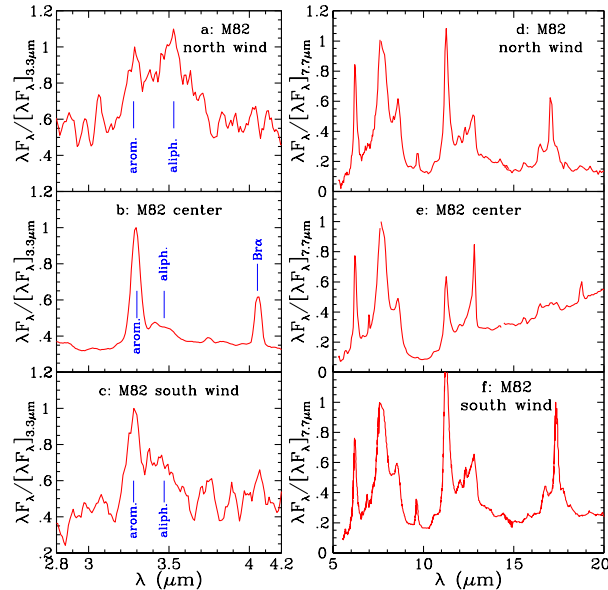
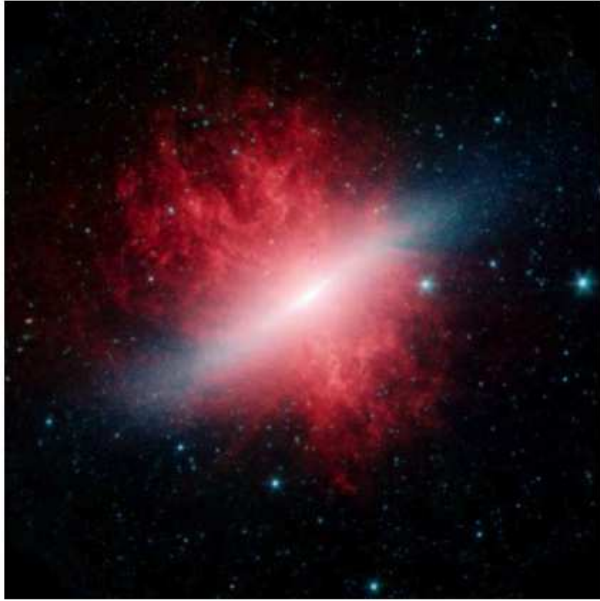


Figure 4: **PAHs in the superwind of M82.** Upper panel: The galaxy is shown as the diffuse bar of blue light. The *Spitzer*/IRAC $8\ \mu\text{m}$ emission, dominated by PAHs, is shown in red. The superwind, emanating from the central starburst region, is evident in the $8\ \mu\text{m}$ emission. The PAH emission is seen all around the galaxy, well beyond the cone defined by the superwind. Lower panel: The near-IR AKARI and mid-IR *Spitzer*/IRS spectra of the north wind (a, d), the center (b, e), and the south wind (c, f) of M82^{88,89}. Most notably, while in the center the $3.3\ \mu\text{m}$ aromatic C–H band is much stronger than the $3.4\ \mu\text{m}$ aliphatic C–H band (b), in the wind the aliphatic band is so pronounced that it even dwarfs the aromatic band (a, c). The intensities of the 11.3 , 12.7 and $17.1\ \mu\text{m}$ bands relative to the 6 – $9\ \mu\text{m}$ bands are stronger in the wind (d, f) than in the center (f). The *Spitzer*/IRAC $8\ \mu\text{m}$ image is adapted from ref.⁸⁷.

protected in clumps¹⁰¹.

Finally, the *Spitzer*/IRS observations of the Galactic bulge also detected PAHs in a local Galactic wind environment¹⁰². The presence of PAHs in the diffuse ionized halo of NGC 891, an edge-on spiral, was also spectroscopically revealed by *Spitzer*/IRS through the observations of the PAH bands at 11.3 , 12.7 , and $16.4\ \mu\text{m}$ ¹⁰³. The detection of PAHs in galaxy halos or superwinds provides valuable insight not only into the destruction and survival of PAHs in hostile environments, but also the mechanism for transporting PAHs from the plane to the halo through supernova explosion, stellar winds, and radiation pressure.

PAHs in galaxy mergers. Galaxy mergers, occurring when two (or more) galaxies collide, could trigger starbursts and lead to the formation of tidal tails stretching $\gtrsim 100\ \text{kpc}$ from the site of the collision¹⁰⁴. Higdon et al.¹⁰⁵ obtained the *Spitzer*/IRS spectra of two faint tidal dwarf galaxies, NGC 5291 N and NGC 5291 S, and detected PAH emission bands at 6.2 , 7.7 , 8.6 , 11.3 , 12.7 , and $16.4\ \mu\text{m}$ which are remarkably similar to those of normal star forming galaxies. In contrast, Haan et al.¹⁰⁶ mapped the PAH bands with *Spitzer*/IRS in eight major merger systems of the Toomre Sequence and found that the spatially resolved $6.2/7.7$ and $11.3/7.7$ interband ratios are often too large to be explainable by the canonical PAH model⁸. Murata et al.¹⁰⁷ examined the relationship of the PAH emission spectra obtained with AKARI with galaxy merger in 55 star-forming galaxies at $z < 0.2$. They found that PAHs are relatively underabundant in merger galaxies than non-merger galaxies and suggested that PAHs are partly destroyed by the intense UV radiation and large-scale shocks during merging processes of galaxies. Based on *Spitzer*/IRS and AKARI data, Onaka et al.¹⁰⁸ detected PAH emission and found that small grains are deficient in the tidal tails of two galaxy mergers, NGC 2782 (Arp 215) and NGC 7727 (Arp 222). They suggested that PAHs are formed from the fragmentation of small grains during merger events.

PAHs in active galactic nuclei. In the harsh environment around active galactic nuclei (AGNs) — rich in extreme UV and soft X-ray photons — PAHs would be destroyed and PAH emission is not expected to be present^{109,110}, as first noticed by Roche et al.¹¹¹ in the ground-based mid-IR spectra of the nuclear regions of active galaxies. Genzel et al.¹¹² proposed to use the strength of the $7.7\ \mu\text{m}$ PAH feature as a discriminator of starburst and AGN activity in ULIRGs, with an aim to determine whether an ULIRG is powered by recently formed massive stars or by a central AGN. However, PAH emission was reportedly detected within $\gtrsim 10\ \text{pc}$ of AGNs, suggesting that PAHs could survive in close proximity to AGNs and be excited by photons from AGNs^{113,114}. Based on the *Spitzer*/IRS spectra of 91 Seyfert galaxies, Tommasin et al.¹¹⁵ also found that, going from AGN-dominated to starburst-dominated objects, the $11.3\ \mu\text{m}$ PAH feature remains almost constant in flux, although its equivalent width increases. They argued that PAHs could survive in the highly ionized medium of AGNs, while the PAH feature appears weaker in the most powerful ones because it is masked by the strong underlying AGN continuum (see their Fig. 14). On the other hand, AKARI and *Spitzer*/IRS observations have shown that PAHs could be destroyed by the intense, hard radiation in starburst galaxies and in the HII regions within star-forming galaxies^{116,117}. Therefore, caution should be taken when one uses the PAH emission as a star formation tracer within a kpc around AGNs or for intense starbursts.

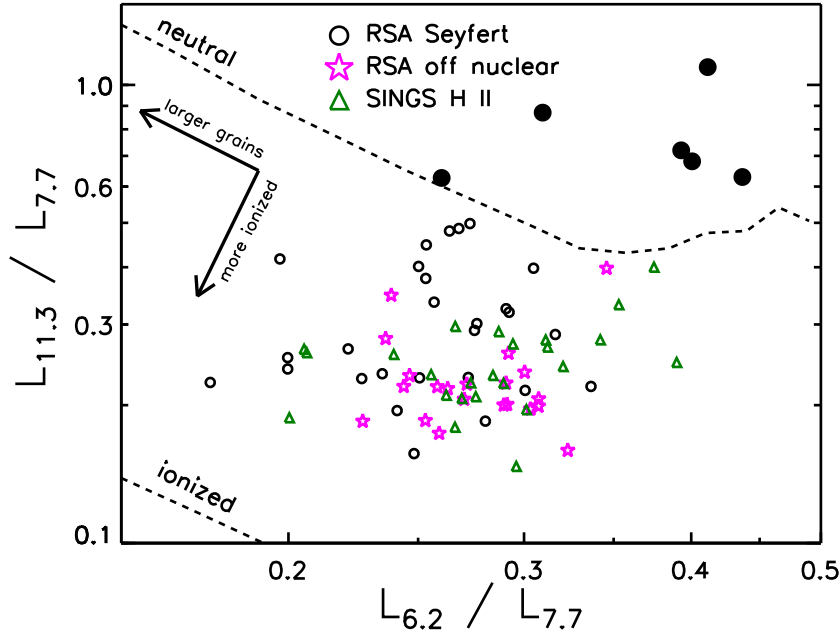


Figure 5: **Relative strengths of the 6.2, 7.7, and 11.3 μm PAH features for Seyfert nuclei (open or filled circles), off-nuclear regions (stars), and HII galaxies (triangles).** The Seyfert galaxies are from the *Revised Shapley-Ames* (RAS) catalog of bright galaxies. $L_{6.2}$, $L_{7.7}$ and $L_{11.3}$ are respectively the power emitted from the 6.2, 7.7 and 11.3 μm features. The dashed lines correspond to predictions of Draine & Li² for completely neutral and completely ionized PAHs with their sizes increasing from right to left; the permitted region of the diagram is bounded by these two lines. The Seyferts highlighted as filled circles all lie beyond the range of model predictions, even for completely neutral molecules. It is likely that heavy processing causes PAHs to have an open, irregular structure and hence a higher H/C ratio and consequently a higher 11.3/7.7 ratio. Adapted from ref.¹¹⁹.

Nevertheless, numerous observations of Seyferts and LINERs with *Spitzer*/IRS have clearly shown that the PAH emission significantly weakens in AGN-hosting galaxy nuclei and the PAH spectra differ considerably from that of star-forming galaxies. More specifically, the PAH bands at 6.2, 7.7, and 8.6 μm of Seyferts and LINERs are often substantially suppressed relative to the 11.3 μm band^{14,118–120}. These trends have been interpreted as the preferential destruction of small PAHs by the hard radiation field of AGNs.

As demonstrated in Fig. 5, the relative strengths of the PAH bands provide powerful diagnostics of the physical and chemical properties of the PAH molecules (e.g., their sizes, charging, and structural characteristics). Both laboratory measurements and quantum-chemical computations have shown that the 3.3 and 11.3 μm features arise primarily from neutral PAHs, while the 6.2, 7.7, and 8.6 μm features are dominated by the emission of ionized PAHs^{28,121,122}. Meanwhile, whether a PAH molecule will be ionized or neutral is controlled by the starlight intensity, electron density and gas temperature^{24,25}. Therefore, the band ratios involving the neutrals and ions, such as the 7.7/11.3 ratio, are useful tools for probing the charging of the emitting molecules and hence for probing the local physical conditions^{8,123}.

By comparing the observed PAH interband ratios with the model expectations for neutral and ionized PAHs, one could determine the PAH size and ionization fraction (i.e., the probability of finding a PAH molecule in a nonzero charge state)^{8,123}. However, as shown in Fig. 5, Diamond-Stanic & Rieke¹¹⁹ found that the 11.3/7.7 ratios of a number of Seyferts lie beyond the range

of model predictions, even for completely neutral PAHs. While large 11.3/7.7 ratios could be produced by large neutral PAHs, they would be expected to have small 6.2/7.7 ratios, inconsistent with the observations. This is because, for a given ionization, larger PAHs tend to emit more at longer wavelengths (i.e., larger 11.3/7.7 ratios and smaller 6.2/7.7 ratios)⁸. The discrepancy between the observed and model-predicted 11.3/7.7 ratios cannot be resolved by nitrogen-containing PAHs. Upon insertion of a nitrogen atom, the 6.2 and 7.7 μm C–C stretches and the 8.6 μm C–H in-plane bending of both neutral and cationic PAHs exhibit a two-fold increase in intensity^{124,125}. Therefore, nitrogen-containing PAHs would produce even lower 11.3/7.7 ratios. We suggest that these extreme 11.3/7.7 ratios could arise from catacondensed PAHs with an open, irregular structure. Catacondensed PAHs have more H atoms (on a per C atom basis) than compact, pericondensed PAHs (e.g., coronene, ovalene, circumcoronene)^{55,63} and hence their emission spectra would have a higher 11.3/7.7 ratio. While the model tracks shown in Fig. 5 for ionized and neutral PAHs at varying sizes were calculated from pericondensed PAHs⁸, heavy processing in the nuclear regions of active galaxies may cause PAHs to have an open, irregular structure and thus a higher 11.3/7.7 ratio. Alternatively, the extreme 11.3/7.7 ratios could result from an inappropriate subtraction of the continuum emission underlying the PAH bands.

PAHs in low-metallicity galaxies. The deficiency or lack of PAHs in low-metallicity galaxies was recognized in the pre-*Spitzer* era. The $\sim 5\text{--}16$ μm mid-IR spectrum of SBS 0335-052, a blue compact dwarf galaxy with an extremely low metallicity

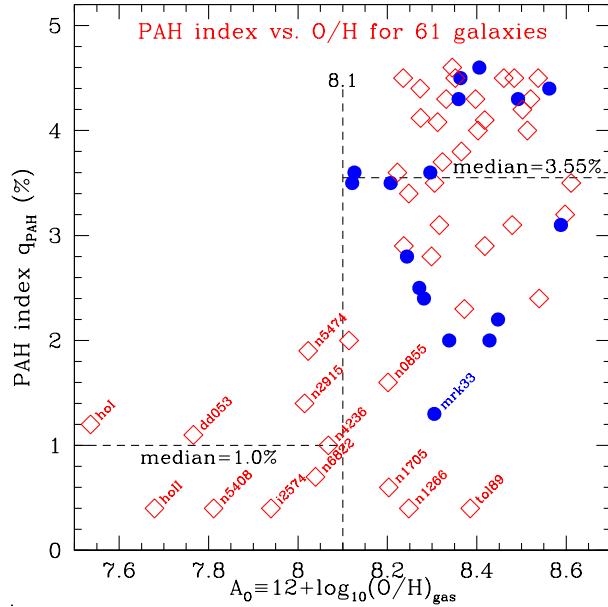


Figure 6: **PAH abundance vs. galaxy metallicity.** The galaxy metallicity $A_{\text{O}} \equiv 12 + \log(\text{O}/\text{H})$ is measured by the gas-phase oxygen abundance (relative to H). The PAH abundance is measured by the mass fraction of dust in PAHs, with an uncertainty of $\sim 0.1\%$. Low metallicity galaxies are always deficient in PAHs. Filled circles are for galaxies having submillimeter data; diamonds are for galaxies lacking submillimeter data. Adapted from ref. ¹³².

of $Z/Z_{\odot} \sim 1/41$, obtained by Thuan et al. ¹²⁶ with the *Circular Variable Filter* (CVF) facility of ISOCAM shows no evidence of PAHs, as later confirmed by the *Spitzer/IRS* observations ¹²⁷. Madden et al. ¹²⁸ performed a more systematic investigation of the ISOCAM CVF mid-IR spectra of a large number of metal-poor dwarf galaxies and found that the PAH features are substantially suppressed. The advent of *Spitzer* not only confirmed the paucity of PAH emission in low-metallicity environments, but more importantly, also established a trend of decreasing PAH emission with metallicity and a threshold in metallicity below which the PAH abundance drops drastically.

The *Spitzer/IRS* spectra of a large number of metal-poor blue compact dwarf galaxies with metallicities from $Z/Z_{\odot} \sim 0.02$ to ~ 0.6 show much weaker PAH features than typical starburst galaxies, with a substantial weakening at $Z/Z_{\odot} \lesssim 0.2$ or $12 + \log(\text{O}/\text{H}) \sim 7.9$ (ref. ^{129,130}). Engelbracht et al. ¹³¹ examined the IRAC $8\mu\text{m}$ and MIPS $24\mu\text{m}$ emission of 34 galaxies spanning two decades in metallicity. They found that $f_{\nu}(8\mu\text{m})/f_{\nu}(24\mu\text{m})$ — the ratio of the $8\mu\text{m}$ emission to the $24\mu\text{m}$ emission — drops abruptly from ~ 0.7 for galaxies with $Z/Z_{\odot} > 1/3$ to ~ 0.08 for galaxies with $Z/Z_{\odot} < 1/5$ – $1/3$. They attributed this drop to a sharp decrease in the $7.7\mu\text{m}$ PAH feature at a threshold metallicity of $12 + \log(\text{O}/\text{H}) \sim 8.2$. By modeling the PAH and dust IR emission of 61 galaxies from the *Spitzer Infrared Nearby Galaxies Survey* (SINGS), Draine et al. ¹³² also found that the PAH abundance shows a sharp change around a threshold in metallicity of $12 + \log(\text{O}/\text{H}) \sim 8.1$ (see Fig. 6), corresponding to $Z/Z_{\odot} \lesssim 0.23$ if we take $Z/Z_{\odot} = 1$ for $12 + \log(\text{O}/\text{H}) = 8.73$ (ref. ¹³³).

With *Spitzer/IRS*, Gordon et al. ¹³⁴ investigated the spatially-resolved PAH features in the face-on spiral galaxy M101 which has one of the largest metallicity gradients. They found that the variation of the strengths of the PAH features correlates better with the radiation field hardness than metallicity. On the contrary, Wu et al. ¹³⁵ found that the PAH emission of 29 faint dwarf galaxies as traced by the *Spitzer/IRAC* [3.6]–[8] color appears to depend more directly on metallicity than radiation hardness.

The exact reason for the deficiency or lack of PAHs in low-metallicity galaxies is not clear. It is generally interpreted as more rapid destruction of PAHs by the more intense and harder UV radiation (as indicated by the fine-structure line ratio of $[\text{NeIII}]/[\text{NeII}]$ in an ISM with reduced shielding by dust. Low-metallicity environments lack sufficient dust grains to shield PAHs from photodissociation by UV radiation, by analogy with the mechanism commonly invoked to explain the deficit of CO emission in low-metallicity galaxies ⁸¹. It could also be due to more effective destruction of PAHs by thermal sputtering in shock-heated gas that cools more slowly because of the reduced metallicity. The reduced PAH abundance in these galaxies might also be due to a deficiency of PAH-producing carbon stars and C-rich planetary nebulae, or a suppressed formation and growth of PAHs in the ISM with low gas-phase C abundances ¹³². Seok et al. ¹³⁶ related the PAH-metallicity dependence to the formation mechanism of PAHs in the ISM. They suggested that interstellar PAHs are formed from the shattering of carbonaceous dust grains in interstellar turbulence. Based on an exploration of the evolution of PAH abundance on a galaxy-evolution time-scale, they found that the formation of PAHs becomes accelerated above certain metallicity where shattering becomes efficient.

The dearth of PAHs in low-metallicity galaxies, if they are truly young, could also result from a delayed production of PAHs by low-mass stars, i.e., PAH-producing carbon stars have not yet evolved off the Main Sequence ¹³⁷. This scenario is supported by the metallicity-dependence of the $7.7\mu\text{m}$ PAH emission of 476 distant galaxies spanning a wide range in metallicity at redshifts $1.37 \lesssim z \lesssim 2.61$. The PAH emission (relative to the total IR emission) is indeed significantly lower in the youngest quartile of the sample with an age of $\lesssim 500$ Myr (ref. ¹³⁸). However, based on a *Spitzer/IRAC* $8\mu\text{m}$ imaging survey of 15 local group dwarf galaxies, Jackson et al. ¹³⁹ found that, although these galaxies are all deficient in PAH emission, they have formed the bulk of their stars more than 2 Gyr ago. Therefore, they argued that the paucity of PAH emission in dwarf galaxies is unlikely due to the shortage of AGB stars.

PAHs in supernova remnants. The PAH spectra of supernova remnants (SNRs) and their implied PAH sizes contain useful information on the shock-processing of PAHs. With *Spitzer/IRS*, Tappe et al. ¹⁴⁰ performed spectroscopic observations of N132D, a young SNR with an age of ~ 2500 yr in the LMC. They reported the detection in N132D of a weak PAH feature at $11.3\mu\text{m}$ and a prominent, broad hump at 15 – $20\mu\text{m}$ attributed to the C-C skeleton bending modes of large PAHs of ~ 4000 C atoms. This was the first ever detection of PAHs in a SNR. The lack of PAH features at 6 – $9\mu\text{m}$ and the large ratio of the 15 – $20\mu\text{m}$ emission to the $11.3\mu\text{m}$ emission indicate that small PAHs could have been rapidly destroyed in the supernova blast wave via thermal sputtering and only larger ones have survived in the shocked environment.

Box 1: Major contributions to PAH astrophysics made by *Spitzer* observations.

- *Spitzer*/IRS observations have provided a complete and unbiased spectroscopic census of the PAH emission bands in the wavelength range of $\sim 5\text{--}20\ \mu\text{m}$, including the discovery of a prominent emission feature centered at $17.1\ \mu\text{m}$ whose intensity is three times as strong as the $16.4\ \mu\text{m}$ feature or nearly half as strong as the $11.3\ \mu\text{m}$ band (see Fig. 1a,c)⁵⁶.
- *Spitzer*/IRS observations have detected PAH emission in external galaxies out to high redshifts $z \gtrsim 4$, indicating the prevalence of complex aromatic organic molecules in the young universe, only $\sim 1.5\ \text{Gyr}$ after the Big Bang⁷⁵.
- With its high sensitivity, *Spitzer* has been able to probe PAH emission in much larger samples spanning much wider varieties of astrophysical regions than ever before, including such hostile environments as AGNs^{118–120}, elliptical galaxies⁸³, galactic outflows or superwinds^{87,88,103}, galaxy mergers¹⁰⁵, low-metallicity galaxies^{127,129–132}, and supernova remnants^{140–142}. In these harsh environments, the PAH spectra are often substantially suppressed in the 6.2 , 7.7 and $8.6\ \mu\text{m}$ bands and enhanced in the $11.3\ \mu\text{m}$ band. The $6\text{--}9\ \mu\text{m}$ PAH emission of protoplanetary disks around T Tauri stars has also been detected, for the first time, by *Spitzer*/IRS^{47–49}.
- The high sensitivity of *Spitzer*/IRS has enabled unprecedented PAH spectral mapping of both Galactic and extragalactic sources, providing valuable information on the spatial variations of the PAH characteristics (e.g., size, charge, structure) and their responses to the changing environments^{51–55}.
- *Spitzer* observations firmly established the PAH-metallicity relation for galaxies spanning over two decades in metallicity and revealed a metallicity threshold of $12 + \log(\text{O}/\text{H}) \sim 8.1$ below which the PAH abundance drops drastically^{129–132}.

In contrast, with AKARI and *Spitzer*/IRS, Seok et al.¹⁴¹ detected the 3.3 , 6.2 , 7.7 and $11.3\ \mu\text{m}$ PAH features in N49, a middle-aged SNR ($\sim 6600\ \text{yr}$) in the LMC, and found that the $6.2/11.3$ and $7.7/11.3$ band ratios imply a predominance of small PAHs. They suggested that, unlike N132D, the PAHs in N49 are possibly associated with the ambient molecular cloud (with which N49 is interacting) where small PAHs could survive from the shock¹⁰¹.

The detection of PAH emission in Galactic SNRs has also been reported with *Spitzer*/IRS¹⁴². Their $\sim 5\text{--}14\ \mu\text{m}$ PAH spectra closely resemble that of Galactic photodissociated regions (PDRs) and star-forming galaxies, but considerably differ from that of N132D in the LMC. Andersen et al.¹⁴² attributed the spectral difference between Galactic SNRs and N132D to their different environments. While many of these Galactic SNRs are in a dense molecular cloud environment with a slow shock, N132D, in a less dense environment, has a strong shock which has effectively destroyed small PAHs.

Concluding Remarks

Spitzer has provided a wealth of spectral and imaging data on the characteristics and spatial distributions of PAHs in a wide variety of astrophysical regions and considerably expanded the field of PAH astrophysics, especially the extragalactic world up to $z \gtrsim 4$ (see Box 1). The PAH model has been successful in explaining the overall spectral profiles and the band patterns observed in various regions in terms of a mixture of neutral and charged PAHs

of different sizes^{8,9,121}. However, longstanding open questions remain, with some of which arising from *Spitzer* observations (see Box 2).

Spitzer/IRS observations of harsh environments such as AGN-hosting Seyfert galaxies¹¹⁹ and galaxy mergers¹⁰⁶ find extreme $11.3/7.7$ band ratios which lie beyond the range of model predictions, even for completely neutral PAHs⁸. Future experimental measurements, quantum chemical computations and theoretical modeling of large catacondensed PAHs with an open, irregular structure will be useful to attest the PAH model. Andrews et al.¹⁴³ suggested that the interstellar PAH family may be dominated by “grandPAHs”, large and hence stable molecules that can survive the harsh conditions of the ISM. However, it is difficult for “grandPAHs” to reconcile with these extreme $11.3/7.7$ band ratios (see Fig. 5).

Another challenge to the PAH model is that, so far, no specific PAH molecule has been identified in the interstellar or circumstellar space¹⁴⁴. Laboratory measurements have shown that individual small PAH molecules (with $\lesssim 25\ \text{C}$ atoms) have strong and narrow absorption features in the UV¹⁴⁵. Attempts to search for these features were made with the *Space Telescope Imaging Spectrograph* on board the *Hubble Space Telescope*¹⁴⁶. However, no such absorption features were seen. We argue that it is natural to expect a large number of distinct PAH species to be present in the ISM, and no single UV band may be strong enough to be identified. The strong interstellar $2175\ \text{\AA}$ extinction feature is likely to be a blend of $\pi\text{--}\pi^*$ absorption bands from the entire population of PAHs^{9,16–19}. Furthermore, internal conversion may lead to extreme broadening of the UV absorption bands in larger PAHs, which may account for absence of recognizable UV absorption features other than the $2175\ \text{\AA}$ bump. Therefore, the lack of identification of any specific PAH is not a fatal problem for the PAH model, at least at this time. As we develop a better knowledge of the gas-phase spectroscopy of larger PAHs, this may change. If the diffuse interstellar bands are electronic transitions of PAHs, they hold great promise for identifying specific PAH molecules, as the electronic transitions are more characteristic of a specific PAH molecule than the mid-IR C–H and C–C vibrational bands, while the latter are mostly representative of functional groups and thus do not allow one to fingerprint individual PAH molecules.

It remains unclear where and how interstellar PAHs are formed. Suggested sources for interstellar PAHs include the formation in the ISM through gas-phase ion-molecule reactions, or through shattering of hydrogenated amorphous carbon dust by grain-grain collisions in interstellar shocks. Also suggested is the formation of PAHs in carbon star outflows followed by subsequent injection into the ISM. Nevertheless, the PAH emission bands are rarely seen in the mid-IR spectra of carbon stars. To our knowledge, only three carbon stars — TU Tau^{147–149}, UV Aur¹⁴⁸, and HD 100764¹⁵⁰ — are known to exhibit PAH emission. It has been suggested that PAHs are present in all C stars but they are simply not excited sufficiently to emit at mid-IR due to lack of UV photons, noting that both TU Tau and UV Aur have a hot companion which emits UV photons^{147–149}. However, it has been shown that the excitation of PAHs do not need very energetic photons, instead, visible and near-IR photons are able to excite PAHs to temperatures high enough to emit the mid-IR bands^{151,152}, in agreement with the detection of PAH emission in regions lack of UV photons, including

Box 2: Puzzling questions about PAHs raised partly from *Spitzer* observations.

- No exact identification of the UIE band carriers has been made yet¹⁴⁴. No specific PAH molecule has been identified in the interstellar or circumstellar space.
- Are interstellar PAHs made in the ISM or condensed in carbon star outflows and subsequently injected into the ISM?
- How do PAHs quantitatively reveal the local physical and chemical conditions and respond to intense, extreme UV and X-ray photons and shocks? How would the chemical structure (e.g., catacondensed vs. pericondensed, aliphaticity vs. aromaticity, dehydrogenation vs. superhydrogenation) of PAHs be affected by photo- and shock-processing? How do the extreme 11.3/7.7 band ratios seen in the *Spitzer*/IRS spectra of AGNs (see Fig. 5) and other harsh environments reflect the size, charging, and structure of PAHs and the processing they have experienced?
- How accurate are PAHs as a SFR indicator? While PAHs are seen in regions within as close as $\gtrsim 10$ pc of AGNs^{113,114}, *Spitzer*/IRS observations have shown that PAHs can be destroyed by intense starbursts^{116,117}. Also, PAH emission does not necessarily trace exclusively young stars as PAHs can also be excited by visible photons^{151–153}.
- What is the nature of the continuum underlying the discrete PAH bands? What is the most appropriate way to subtract the continuum to measure the PAH emission (which is crucial for accurately determining the SFRs and the PAH band ratios)?
- Are PAHs related to other unexplained interstellar phenomena (e.g., the 2175 Å extinction bump, the diffuse interstellar bands, the blue and extended red photoluminescence emission, and the “anomalous microwave emission”), other interstellar carbon species (e.g., C₆₀, carbon chains, and possibly graphene and carbon nanotubes)^{180–183}, and the chemical complexity of the Universe including the formation of H₂ and their role as a viable sink of interstellar deuterium¹⁶⁸?
- How do PAHs evolve from the ISM to prestellar nebulae, protoplanetary disks, comets, and meteorites? Why PAHs are not seen in embedded protostars, the early phases of star formation? Why are PAHs generally smaller in meteorites¹⁸⁴ and T Tauri disks⁴⁹ than that in the ISM?

vdB 133, a reflection nebula illuminated by a F5 Iab star of effective temperature $T_{\star} \approx 6800$ K¹⁵³, HD 100764, a C-rich red giant of $T_{\star} \approx 4850$ K¹⁵⁰, and HD 233517, an O-rich red giant of $T_{\star} \approx 4475$ K¹⁵⁴.

The distribution of PAHs in the SMC, derived from the *Spitzer*/IRAC photometric mapping data, does not follow that of C-rich AGB stars, instead, it correlates with molecular gas as traced by CO (ref.¹⁵⁵). This suggests that PAHs may be forming in molecular clouds. In contrast, the distribution of PAHs in the LMC, also derived from the *Spitzer*/IRAC mapping data, is enhanced both in molecular clouds and in the stellar bar, which hosts the highest concentration of AGB stars¹⁵⁶. The association of PAH emission with the stellar bar in the LMC was considered as evidence for C-rich AGB stars as a PAH source. However, we argue that, if PAHs are formed from the fragmentation of carbonaceous dust grains which were condensed in AGB stars and subsequently injected into the ISM, one would also expect the distribution of PAHs to be enhanced in the stellar bar. With the Faint Object Infrared Camera (FORCAST) onboard the Stratospheric Observatory for Infrared Astronomy (SOFIA), the mid-IR imaging observations of NGC 7027, a planetary nebula of age ~ 1000 yr, suggested rapid PAH formation along the outflow via grain-grain collisions in the post-shock environment of the dense photodissociation region and molecular envelope¹⁵⁷. With the upcoming JWST, smaller spatial scales can be probed; spectral mapping in the PAH bands of the outflows of C-rich AGB stars and planetary nebulae will be valuable for exploring the origin and evolution of PAHs.

The emission continuum underlying the discrete PAH features is pervasive¹⁵⁸ and its nature remains unclear¹⁵⁹. It is noteworthy that the reliability of PAH emission as an effective SFR indicator relies on the appropriate subtraction of the underlying continuum for which no consensus has yet been reached^{14,160–163}. The observed band ratios (e.g., the extreme 11.3/7.7 ratios seen in hostile environments) used to derive the PAH size, charge and structure and the local physical and chemical conditions also depend on how the continuum is defined and subtracted. The con-

tinuum emission was posited to be related to the anharmonicity of highly vibrationally excited PAHs⁷, some specific PAH species (e.g., tubular PAHs) with a zero bandgap¹⁰, or energetically processed PAHs¹⁶⁴. Kwok & Zhang¹⁴⁴ proposed that organic nanoparticles with a mixed aromatic-aliphatic structure could be responsible for both the PAH emission bands and the underlying continuum. However, the 3.3 μm emission feature and the underlying continuum emission at ~ 2 μm in NGC 2023, a reflection nebula, are spatially separated, suggesting the 3.3 μm feature and the underlying continuum do not share the same carrier¹⁶⁵. Future spatially resolved observations with JWST and SPICA that can map the two components will provide insight into their physical separations and chemical carriers.

Compared with *Spitzer*, JWST will have more than an order of magnitude increase in sensitivity and spatial resolution as well as a broader wavelength coverage in the near-IR. While the 3.3 μm C–H stretch and the accompanying satellite features at 3.4–3.6 μm are beyond the wavelength range of *Spitzer*/IRS, it is expected that JWST, with its *Near InfraRed Spectrograph* (NIRSpec) operating at 0.6–5 μm , will be able to scrutinize these bands so as to study the chemical structures (e.g., methylation, superhydrogenation, and anharmonicity) of the smallest PAHs and their environmental dependence. Moreover, JWST/NIRSpec will be ideal for searching for the overtone band at ~ 1.6 –1.8 μm of the 3.3 μm feature of small PAHs, providing valuable insights into the PAH fluorescence process^{166,167}. Furthermore, the C–D stretch at ~ 4.4 μm of deuterated PAHs will be of particular interest. PAHs could be a major reservoir of deuterium in the ISM. PAHs of intermediate size (with $\lesssim 100$ C atoms) are expected to become deuterium enriched in the ISM through the selective loss of hydrogen during photodissociation events¹⁶⁸. While ISO/SWS and AKARI observations have reported the tentative detection of the C–D bands at 4.4 and 4.65 μm in the Orion Bar and M17 PDRs^{169,170} and HII regions¹⁷¹, the unique high sensitivity of JWST/NIRSpec will place the detection of deuterated PAHs on firm ground and enable far more detailed band analysis than previously possible.

The high sensitivity and high spatial resolution capabilities of JWST and SPICA will open up an IR window unexplored by *Spitzer* and unmatched by *ISO* observations. With JWST and SPICA aided by laboratory studies, quantum chemical computations, and theoretical modeling, the future of PAH astrophysics will be even more promising!

1. Gillett, F.C., Forrest, W.J. & Merrill, K.M. 8–13 μm spectra of NGC 7027, BD+30 3639, and NGC 6572. *Astrophys. J.* **183**, 87–93 (1973).
2. Merrill, K.M., Soifer, B.T. & Russell, R.W. The 2–4 μm spectrum of NGC 7027. *Astrophys. J.* **200**, L37–L39 (1975).
3. Russell, R.W., Soifer, B.T. & Willner, S.P. The 4–8 μm spectrum of NGC 7027. *Astrophys. J.* **217**, L149–L153 (1977).
4. Willner, S.P., Soifer, B.T., Russell, R.W. Joyce, R.R. & Gillett, F.C. 2–8 μm spectrophotometry of M82. *Astrophys. J.* **217**, L121–L124 (1977).
5. Léger, A. & Puget, J.L. Identification of the “unidentified” IR emission features of interstellar dust? *Astron. Astrophys.* **137**, L5–L8 (1984).
6. Allamandola, L.J., Tielens, A.G.G.M. & Baker, J.R. Polycyclic aromatic hydrocarbons and the unidentified infrared emission bands: Auto exhaust along the Milky Way. *Astrophys. J.* **290**, L25–L28 (1985).
7. Allamandola, L.J., Tielens, A.G.G.M. & Baker, J.R. Interstellar polycyclic aromatic hydrocarbons: The infrared emission bands, the excitation/emission mechanism, and the astrophysical implications. *Astrophys. J. Supp.* **71**, 733–775 (1989).
8. Draine, B.T. & Li, A. Infrared emission from interstellar dust. I. Stochastic heating of small grains. *Astrophys. J.* **551**, 807–824 (2001).
9. Li, A. & Draine, B.T. Infrared emission from interstellar dust. II. The diffuse interstellar medium. *Astrophys. J.* **554**, 778–802 (2001).
10. Draine, B.T. & Li, A. Infrared emission from interstellar dust. IV. The silicate-graphite-PAH model in the post-*Spitzer* era. *Astrophys. J.* **657**, 810–837 (2007).
11. Zubko, V., Dwek, E. & Arendt, R.G. Interstellar dust models consistent with extinction, emission, and abundance constraints. *Astrophys. J. Supp.* **152**, 211–249 (2004).
12. Siebenmorgen, R., Voshchinnikov, N.V. & Bagnulo, S. Dust in the diffuse interstellar medium. Extinction, emission, linear and circular polarisation. *Astron. Astrophys.* **561**, A82 (2014).
13. Jones, A.P., Köhler, M., Ysard, N., Bocchio, M. & Verstraete, L. The global dust modelling framework THEMIS. *Astron. Astrophys.* **602**, A46 (2017).
14. Smith, J.D.T., *et al.* The mid-infrared spectrum of star-forming galaxies: Global properties of polycyclic aromatic hydrocarbon emission. *Astrophys. J.* **656**, 770–791 (2007).
15. Tielens, A. G. G. M. Interstellar polycyclic aromatic hydrocarbon molecules. *ARA&A* **46**, 289–337 (2008).
16. Joblin, C., Léger, A. & Martin, P. Contribution of polycyclic aromatic hydrocarbon molecules to the interstellar extinction curve. *Astrophys. J.* **393**, L79–L82 (1992).
17. Cecchi-Pestellini, C., Mallocci, G., Joblin, C. & Williams, D.A. The role of the charge state of PAHs in ultraviolet extinction. *Astron. Astrophys.* **486**, 25–29 (2008).
18. Mulas, G., Zonca, A., Casu, S. & Cecchi-Pestellini, C. Modeling Galactic extinction with dust and “real” polycyclic aromatic hydrocarbons. *Astrophys. J. Supp.* **207**, 7 (2013).
19. Steglich, M., Jäger, C., Rouillé, G., Huisken, F., Mutschke, H. & Henning, Th. Electronic spectroscopy of medium-sized polycyclic aromatic hydrocarbons: Implications for the carriers of the 2175 Å UV bump. *Astrophys. J.* **712**, L16–L20 (2011).
20. Salama, F., *et al.* Polycyclic aromatic hydrocarbons and the diffuse interstellar bands: A survey. *Astrophys. J.* **728**, 154 (2011).
21. Witt, A.N. Blue luminescence and extended red emission: Possible connections to the diffuse interstellar bands. *IAUS* **297**, 173–179 (2014).
22. Draine, B.T. Interstellar dust grains. *ARA&A* **41**, 241–289 (2003).
23. Dickinson, C., *et al.* The state-of-play of anomalous microwave emission (AME) research. *New Astron. Rev.* **80**, 1–28 (2018).
24. Bakes, E. & Tielens, A.G.G.M. The photoelectric heating mechanism for very small graphitic grains and polycyclic aromatic hydrocarbons. *Astrophys. J.* **427**, 822–838 (1994).
25. Weingartner, J.C. & Draine, B.T. Photoelectric emission from interstellar dust: Grain charging and gas heating. *Astrophys. J. Supp.* **134**, 263–282 (2001).
26. Kamp, I. & Dullemond, C.P. The gas temperature in the surface layers of protoplanetary disks. *Astrophys. J.* **615**, 991–999 (2004).
27. Verstraete, L. The role of PAHs in the physics of the interstellar medium. *EAS Publ. Ser.* **46**, 415–426 (2011).
28. Hudgins, D.M. & Allamandola, L.J. Steps toward identifying PAHs: A summary of some recent results. *IAUS* **231**, 443–454 (2005).
29. Sellgren, K., Werner, M.W. & Dinerstein, H.L. Extended near-infrared emission from visual reflection nebulae. *Astrophys. J.* **271**, L13–L17 (1983).
30. Greenberg, J.M. Interstellar grains. In *Stars and stellar systems*. ed. B.M. Middlehurst & L.H. Aller. (Chicago: Univ. Chicago Press) **7**, 221–364 (1968).
31. Sellgren, K. The near-infrared continuum emission of visual reflection nebulae. *Astrophys. J.* **277**, 623–633 (1984).
32. Geballe, T.R., Lacy, J.H., Persson, S.E., McGregor, P.J. & Soifer, B.T. Spectroscopy of the 3 μm emission features. *Astrophys. J.* **292**, 500–505 (1985).
33. Jourdain de Muizon, M., Geballe, T.R., d’Hendecourt, L.B. & Baas, F. New emission features in the infrared spectra of two IRAS sources. *Astrophys. J.* **306**, L105–L108 (1986).
34. Joblin, C., Tielens, A.G.G.M., Allamandola, L.J. & Geballe, T.R. Spatial variation of the 3.29 and 3.40 μm emission bands within reflection nebulae and the photochemical evolution of methylated polycyclic aromatic hydrocarbons. *Astrophys. J.* **458**, 610–620 (1996).
35. Cohen, M., Tielens, A.G.G.M. & Allamandola, L.J. A new emission feature in IRAS spectra and the polycyclic aromatic hydrocarbon spectrum. *Astrophys. J.* **299**, L93–L97 (1985).
36. Tokunaga, A.T. A summary of the “UIR” bands. *ASP Conf. Ser.* **124**, 149–160 (1997).
37. Cohen, M., *et al.* The infrared emission bands. III. Southern IRAS sources. *Astrophys. J.* **341**, 246–269 (1989).
38. Peeters, E., Allamandola, L.J., Hudgins, D.M., Hony, S. & Tielens, A.G.G.M. The unidentified infrared features after ISO. *ASP Conf. Ser.* **309**, 141–162 (2004).
39. Moutou, C., Verstraete, L., Léger, A., Sellgren, K. & Schmidt, W. New PAH mode at 16.4 μm . *Astron. Astrophys.* **354**, L17–L20 (2000).
40. Schutte, W.A., *et al.* ISO-SWS observations of infrared absorption bands of the diffuse interstellar medium: The 6.2 μm feature of aromatic compounds. *Astron. Astrophys.* **337**, 261–274 (1998).
41. Chiar, J.E., *et al.* The composition and distribution of dust along the line of sight toward the Galactic center. *Astrophys. J.* **537**, 749–762 (2000).
42. Peeters, E. *et al.* The rich 6 to 9 μm spectrum of interstellar PAHs. *Astron. Astrophys.* **390**, 1089–1113 (2002).
43. Mattila, K., *et al.* Spectrophotometry of UIR bands in the diffuse emission of the Galactic disk. *Astron. Astrophys.* **315**, L353–L356 (2000).
44. Onaka, T., Yamamura, I., Tanabe, T., Roellig, T. L. & Yuen, L. Detection of the mid-infrared unidentified bands in the diffuse Galactic emission by IRTS. *PASJ* **48**, L59–L63 (1996).
45. Tanaka, M., *et al.* IRTS observation of the unidentified 3.3 μm band in the diffuse Galactic emission. *PASJ* **48**, L53–L57 (1996).
46. Siebenmorgen, R., Prusti, T., Natta, A. & Müller, T.G. Mid infrared emission of nearby Herbig Ae/Be stars. *Astron. Astrophys.* **361**, 258–264 (2006).
47. Furlan, E., *et al.* A survey and analysis of *Spitzer* Infrared Spectrograph spectra of T Tauri stars in Taurus. *Astrophys. J. Supp.* **165**, 568–605 (2006).
48. Geers, V.C., *et al.* C2D *Spitzer*-IRS spectra of disks around T Tauri stars. II. PAH emission features. *Astron. Astrophys.* **459**, 545–556 (2006).
49. Seok, J.Y. & Li, A. Polycyclic aromatic hydrocarbons in protoplanetary disks around Herbig Ae/Be and T Tauri stars. *Astrophys. J.* **835**, 291 (2017).

50. Ingalls, J.G., *et al.* *Spitzer Infrared Spectrograph* detection of molecular hydrogen rotational emission towards translucent clouds. *Astrophys. J.* **743**, 174 (2011).
51. Sandstrom, K.M., *et al.* The *Spitzer* spectroscopic survey of the Small Magellanic Cloud (S4MC): Probing the physical state of polycyclic aromatic hydrocarbons in a low-metallicity environment. *Astrophys. J.* **744**, 20 (2012).
52. Hemachandra, D., *et al.* Mid-infrared spectroscopy of the Andromeda galaxy. *Astron. Astrophys.* **454**, 818–830 (2015).
53. Boersma, C., Rubin, R.H. & Allamandola, L.J. Spatial analysis of the polycyclic aromatic hydrocarbon features southeast of the Orion Bar. *Astrophys. J.* **753**, 168 (2012).
54. Boersma, C., Bregman, J. & Allamandola, L.J. Properties of polycyclic aromatic hydrocarbons in the northwest photon dominated region of NGC 7023. III. Quantifying the traditional proxy for PAH charge and assessing its role. *Astrophys. J.* **806**, 121 (2015).
55. Shannon, M.J., Stock, D.J. & Peeters, E. Interpreting the subtle spectral variations of the 11.2 and 12.7 μm polycyclic aromatic hydrocarbon bands. *Astrophys. J.* **824**, 111 (2016).
56. Smith, J.D.T., *et al.* Mid-infrared IRS spectroscopy of NGC 7331: A first look at the *Spitzer Infrared Nearby Galaxies Survey* (SINGS) legacy. *Astrophys. J. Supp.* **154**, 199–203 (2004).
57. Werner, M.W., *et al.* New infrared emission features and spectral variations in NGC 7023. *Astrophys. J. Supp.* **154**, 309–314 (2004).
58. Beintema, D.A., *et al.* The rich spectrum of circumstellar PAHs. *Astron. Astrophys.* **315**, L369–L372 (1996).
59. van Kerckhoven, C., *et al.* The C-C-C bending modes of PAHs: A new emission plateau from 15 to 20 μm . *Astrophys. J. Supp.* **357**, 1013–1019 (2000).
60. Cami, J., Bernard-Salas, J., Peeters, E. & Malek, S.E. Detection of C_{60} and C_{70} in a young planetary nebula. *Science* **329**, 1180–1182 (2010).
61. Sellgren, K. *et al.* C_{60} in reflection nebulae. *Astrophys. J.* **722**, L54–L57 (2010).
62. Witteborn, F.C., *et al.* New emission features in the 11–13 μm region and their relationship to polycyclic aromatic hydrocarbons. *Astrophys. J.* **341**, 270–277 (1989).
63. Hony, S., van Kerckhoven, C., Peeters, E., Tielens, A.G.G.M., Hudgins, D.M. & Allamandola, L.J. The CH out-of-plane bending modes of PAH molecules in astrophysical environments. *Astron. Astrophys.* **370**, 1030–1043 (2001).
64. Hudgins, D.M. & Allamandola, L.J. Interstellar PAH emission in the 11–14 μm region: New insights from laboratory data and a tracer of ionized PAHs. *Astrophys. J.* **516**, L41–L44 (1999).
65. Matsuura, M., *et al.* *Spitzer Space Telescope* spectra of post-AGB stars in the Large Magellanic Cloud – Polycyclic aromatic hydrocarbons at low metallicities. *Mon. Not. R. Astron. Soc.* **439**, 1472–1493 (2014).
66. Sloan, G.C., *et al.* Carbon-rich dust past the asymptotic giant branch: Aliphatics, aromatics, and fullerenes in the Magellanic Clouds. *Astrophys. J.* **791**, 28 (2014).
67. Hudgins, D.M., Bauschlicher, J.C.W., & Allamandola, L.J. Variations in the peak position of the 6.2 μm interstellar emission feature: A tracer of N in the interstellar polycyclic aromatic hydrocarbon population. *Astrophys. J.* **632**, 316–332 (2005).
68. Canelo, C.M., Friaça, A.C.S., Sales, D.A., Pastoriza, M.G. & Ruschel-Dutra, D. Variations in the 6.2 μm emission profile in starburst-dominated galaxies: A signature of polycyclic aromatic nitrogen heterocycles (PANHs)? *Mon. Not. R. Astron. Soc.* **475**, 3746–3763 (2018).
69. Berné, O., *et al.* Analysis of the emission of very small dust particles from *Spitzer* spectro-imagery data using blind signal separation methods. *Astron. Astrophys.* **469**, 575–586 (2007).
70. Povich, M.S., *et al.* A Multiwavelength study of M17: The spectral energy distribution and PAH emission morphology of a massive star formation region. **660**, 346–362 (2007).
71. Elbaz, D., Le Floc'h, E., Dole, H. Marcellac, D. Observational evidence for the presence of PAHs in distant Luminous Infrared Galaxies using ISO and *Spitzer*. *Astron. Astrophys.* **434**, L1–L4 (2004).
72. Yan, L., *et al.* *Spitzer* detection of polycyclic aromatic hydrocarbon and silicate dust features in the mid-infrared spectra of $z \sim 2$ ultraluminous infrared galaxies. *Astrophys. J.* **628**, 604–610 (2005).
73. Lutz, D., *et al.* Mid-infrared spectroscopy of two luminous submillimeter galaxies at $z \sim 2.8$. *Astrophys. J.* **625**, L83–L86 (2005).
74. Siana, B., *et al.* Detection of far-infrared and polycyclic aromatic hydrocarbon emission from the Cosmic Eye: Probing the dust and star formation of Lyman break galaxies. *Astrophys. J.* **698**, 1273–1281 (2009).
75. Riechers, D.A., *et al.* Polycyclic aromatic hydrocarbon and mid-infrared continuum emission in a $z > 4$ submillimeter galaxy. *Astrophys. J.* **786**, 31 (2014).
76. Bernstein, M.P., *et al.* UV irradiation of polycyclic aromatic hydrocarbons in ices: Production of alcohols, quinones, and ethers. *Science* **283**, 1158–1138 (1999).
77. Kwok, S. Complex organics in space from Solar System to distant galaxies. *Astron. Astrophys. Rev.* **24**, 8 (2016).
78. Shipley, H.V., *et al.* A new star formation rate calibration from polycyclic aromatic hydrocarbon emission features and application to high-redshift galaxies. *Astrophys. J.* **818**, 60 (2016).
79. Pope, A., *et al.* Mid-infrared spectral diagnosis of submillimeter galaxies. *Astrophys. J.* **675**, 1171–1193 (2008).
80. Calzetti, D., *et al.* The calibration of mid-infrared star formation rate indicators. *Astrophys. J.* **666**, 870–895 (2007).
81. Xie, Y. & Ho, L.C. A new calibration of star formation rate in galaxies based on polycyclic aromatic hydrocarbon emission. *Astrophys. J.* **884**, 136 (2019).
82. Kaneda, H., *et al.* Unbiased large spectroscopic surveys of galaxies selected by SPICA using dust bands. *Publ. Astron. Soc. Aust.* **34**, e059 (2017).
83. Kaneda, H., Onaka, T. & Sakon, I. Detection of PAH emission features from nearby elliptical galaxies with the *Spitzer Infrared Spectrograph*. *Astrophys. J.* **632**, L83–L86 (2005).
84. Kaneda, H., Onaka, T., Sakon, I., Kitayama, T., Okada, Y. & Suzuki, T. Properties of polycyclic aromatic hydrocarbons in local elliptical galaxies revealed by the *Infrared Spectrograph on Spitzer*. *Astrophys. J.* **684**, 270–281 (2008).
85. Vega, O. *et al.* Unusual PAH emission in nearby early-type galaxies: A signature of an intermediate-age stellar population? *Astrophys. J.* **721**, 1090–1104 (2010).
86. Irwin, J.A. & Madden, S.C. Discovery of PAHs in the halo of NGC 5907. *Astron. Astrophys.* **445**, 123–141 (2005).
87. Engelbracht, C.W., *et al.* Extended mid-infrared aromatic feature emission in M82. *Astrophys. J.* **642**, 127–132 (2006).
88. Beirão, P., *et al.* Spatially resolved *Spitzer*-IRS spectral maps of the superwind in M82. *Mon. Not. R. Astron. Soc.* **451**, 2640–2655 (2015).
89. Yamagishi, M. *et al.* AKARI near-infrared spectroscopy of the aromatic and aliphatic hydrocarbon emission features in the galactic superwind of M82. *Astron. Astrophys.* **541**, A10 (2012).
90. Schutte, W.A., Tielens, A.G.G.M. & Allamandola, L.J. Theoretical modeling of the infrared fluorescence from interstellar polycyclic aromatic hydrocarbons. *Astrophys. J.* **415**, 397–414 (1993).
91. Bernstein, M.P., Sandford, S.A. & Allamandola, L.J. Hydrogenated polycyclic aromatic hydrocarbons and the 2940 and 2850 wavenumber (3.40 and 3.51 μm) infrared emission features. *Astrophys. J.* **472**, L127–L130 (1996).
92. Sandford, S.A. The infrared spectra of polycyclic aromatic hydrocarbons with excess peripheral H atoms (H_n -PAHs) and their relation to the 3.4 and 6.9 μm PAH emission features. *Astrophys. J. Supp.* **205**, 8 (2013).
93. Steglich, M. *et al.* The abundances of hydrocarbon functional groups in the interstellar medium inferred from laboratory spectra of hydrogenated and methylated polycyclic aromatic hydrocarbons. *Astrophys. J. Supp.* **208**, 26 (2013).
94. Yang, X.J., Li, A. & Glaser, R. Superhydrogenated polycyclic aromatic hydrocarbon molecules: Vibrational spectra in the infrared. *Astrophys. J. Supp.* **247**, 1 (2020).
95. Baker, J.R. Allamandola, L.J. & Tielens A.G.G.M. Anharmonicity and the interstellar polycyclic aromatic hydrocarbon infrared emission spectrum. *Astrophys. J.* **315**, L61–L65 (1987).
96. Maltseva, E., *et al.* High-resolution IR absorption spectroscopy of polycyclic aromatic hydrocarbons in the 3 μm region: Role of periphery. *Astrophys. J. Supp.* **831**, 58 (2016).
97. Li, A. & Draine, B.T. The carriers of the interstellar unidentified infrared emission features: Aromatic or aliphatic? *Astrophys. J.* **760**, L35 (2012).

98. Yang, X.J., Glaser, R., Li, A. & Zhong, J.X. The carriers of the interstellar unidentified infrared emission features: Constraints from the interstellar C-H stretching features at 3.2–3.5 μm . *Astrophys. J.* **776**, 110 (2013).
99. Yang, X.J., Glaser, R., Li, A. & Zhong, J.X. The carriers of the unidentified infrared emission features: Clues from polycyclic aromatic hydrocarbons with aliphatic sidegroups. *New Astron. Rev.* **77**, 1–22 (2016).
100. Yang, X.J., Glaser, R., Li, A. & Zhong, J.X. On the aliphatic versus aromatic content of the carriers of the 'unidentified' infrared emission features. *Mon. Not. R. Astron. Soc.* **462**, 1551–1562 (2016).
101. Micelotta, E.R., Jones, A.P. & Tielens, A.G.G.M. Polycyclic aromatic hydrocarbon processing in interstellar shocks. *Astron. Astrophys.* **510**, A36 (2010).
102. Shannon, M.J., Peeters, E., Cami, J. & Blommaert, J. A.D.L. Polycyclic aromatic hydrocarbon emission toward the Galactic bulge. *Astrophys. J.* **855**, 32 (2018).
103. Rand, R.J., Wood, K. & Benjamin, R.A. Infrared spectroscopy of the diffuse ionized halo of NGC 891. *Astrophys. J.* **680**, 263–275 (2008).
104. Sanders, D.B. & Mirabel, I.F. Luminous infrared galaxies. *ARA&A* **34**, 749–792 (1996).
105. Higdon, S.J., Higdon, J.L. & Marshall, J. First detection of PAHs and warm molecular hydrogen in tidal dwarf galaxies. *Astrophys. J.* **640**, 768–783 (2006).
106. Haan, S., *et al.* *Spitzer* IRS spectral mapping of the Toomre Sequence: Spatial variations of PAH, gas, and dust properties in nearby major mergers. *Astrophys. J. Supp.* **197**, 27 (2011).
107. Murata, K.L., *et al.* A relationship of polycyclic aromatic hydrocarbon features with galaxy merger in star-forming galaxies at $z < 0.2$. *Mon. Not. R. Astron. Soc.* **472**, 39–50 (2017).
108. Onaka, T., *et al.* Near-infrared to mid-infrared observations of galaxy mergers: NGC 2782 and NGC 7727. *Astrophys. J.* **853**, 31 (2018).
109. Voit, G. M. Destruction and survival of polycyclic aromatic hydrocarbons in active galaxies. *Mon. Not. R. Astron. Soc.* **258**, 841–848 (1992).
110. Siebenmorgen, R., Krügel, E. & Spoon, H.W.W. Mid-infrared emission of galactic nuclei. TIMM12 versus ISO observations and models. *Astron. Astrophys.* **414**, 123–139 (2004).
111. Roche, P.F., Aitken, D.K., Smith, C.H. & Ward, M.J. An atlas of mid-infrared spectra of galaxy nuclei. *Mon. Not. R. Astron. Soc.* **248**, 606–629 (1991).
112. Genezel, R., *et al.* What powers ultraluminous IRAS galaxies? *Astrophys. J.* **498**, 579–605 (1998).
113. Esquej, C. W., *et al.* Nuclear star formation activity and black hole accretion in nearby Seyfert galaxies. *Astrophys. J.* **780**, 86–100 (2014).
114. Jensen, J.J., *et al.* PAH features within few hundred parsecs of active galactic nuclei. *Mon. Not. R. Astron. Soc.* **470**, 3071–3094 (2017).
115. Tommasin, S., *et al.* *Spitzer*-IRS high-resolution spectroscopy of the 12 μm Seyfert galaxies. II. Results for the complete data set. *Astrophys. J.* **709**, 1257–1283 (2010).
116. Murata, K.L., *et al.* Evolution of the fraction of clumpy galaxies at $0.2 < z < 1.0$ in the COSMOS field. *Astrophys. J.* **786**, 15 (2014).
117. Maragkoudakis, A., *et al.* PAHs and star formation in the HII regions of nearby galaxies M83 and M33. *Mon. Not. R. Astron. Soc.* **481**, 5370–5393 (2018).
118. O'Dowd, M.J., *et al.* Polycyclic aromatic hydrocarbons in galaxies at $z \sim 0.1$: The effect of star formation and active galactic nuclei. *Astrophys. J.* **705**, 885–898 (2009).
119. Diamond-Stanic, A.M. & Rieke, G.H. The effect of active galactic nuclei on the mid-infrared aromatic features. *Astrophys. J.* **724**, 140–153 (2010).
120. Wu, Y., *et al.* Infrared luminosities and aromatic features in the 24 μm flux-limited sample of 5MUSES. *Astrophys. J.* **723**, 895–914 (2010).
121. Allamandola, L.J., Hudgins, D.M., & Sandford, S.A. Modeling the unidentified infrared emission with combinations of polycyclic aromatic hydrocarbons. *Astrophys. J.* **511**, L115–L119 (1999).
122. Bauschlicher, C.W., Ricca, A., Boersma, C. & Allamandola, L.J. The NASA Ames PAH IR spectroscopic database: Computational version 3.00 with updated content and the introduction of multiple scaling factors. *Astrophys. J. Supp.* **234**, 32 (2018).
123. Galliano, F., Madden, S.C., Tielens, A.G.G.M., Peeters, E. & Jones, A.P. Variations of the mid-IR aromatic features inside and among galaxies. *Astrophys. J.* **679**, 310–345 (2008).
124. Mattioda, A.L., Hudgins, D.M., Bauschlicher, C.W., Rosi, M. & Allamandola, L.J. Infrared spectroscopy of matrix-isolated polycyclic aromatic compounds and their ions. 6. Polycyclic aromatic nitrogen heterocycles. *J. Phys. Chem. A* **107**, 1486–1498 (2003).
125. Mattioda, A.L., *et al.* Infrared spectroscopy of matrix-isolated neutral polycyclic aromatic nitrogen heterocycles: The acridine series. *Spectrochim. Acta A* **181**, 286–308 (2017).
126. Thuan, T.X., Sauvage, M. & Madden, S. Dust in an extremely metal-poor galaxy: Mid-infrared observations of SBS 0335-052. *Astrophys. J.* **516**, 783–787 (1999).
127. Houck, J.R., *et al.* The extraordinary mid-infrared spectrum of the blue compact dwarf galaxy SBS 0335-052. *Astrophys. J. Supp.* **154**, 211–214 (2004).
128. Madden, S.C., Galliano, F., Jones, A.P. & Sauvage, M. ISM properties in low-metallicity environments. *Astron. Astrophys.* **446** 877–896 (2006).
129. Wu, Y., *et al.* Mid-infrared properties of low-metallicity blue compact dwarf galaxies from the *Spitzer* Infrared Spectrograph. *Astrophys. J.* **639**, 157–172 (2006).
130. Hunt, L.K., Thuan, T.X., Izotov, Y.I. & Sauvage, M. The *Spitzer* view of low-metallicity star formation. III. Fine-structure lines, aromatic features, and molecules. *Astrophys. J.* **712**, 164–187 (2010).
131. Engelbracht, C.W., *et al.* Metallicity effects on mid-infrared colors and the 8 μm PAH emission in galaxies. *Astrophys. J.* **628**, 29–32 (2005).
132. Draine, B.T., *et al.* Dust masses, PAH abundances, and starlight intensities in the SINGS galaxy sample. *Astrophys. J.* **663**, 866–894 (2007).
133. Asplund, M., Grevesse, N., Sauval, A.J. & Scott, P. The chemical composition of the Sun. *ARA&A* **47**, 481–522 (2009).
134. Gordon, K.D. *et al.* The behavior of the aromatic features in M101 HII regions: Evidence for dust processing. *Astrophys. J.* **682**, 336–354 (2008).
135. Wu, R., Hogg, D.W. & Moustakas, J. The aromatic features in very faint dwarf galaxies. *Astrophys. J.* **730**, 111 (2011).
136. Seok, J.Y., Hirashita, H. & Asano, R.S. Formation history of polycyclic aromatic hydrocarbons in galaxies. *Mon. Not. R. Astron. Soc.* **439**, 2186–2196 (2014).
137. Galliano, F., Dwek, E. & Charnial, P. Stellar evolutionary effects on the abundances of polycyclic aromatic hydrocarbons and supernova-condensed dust in galaxies. *Astrophys. J.* **672**, 214–243 (2008).
138. Shivaeei, I., *et al.* The MOSDEF survey: Metallicity dependence of PAH emission at high redshift and implications for 24 μm inferred IR luminosities and star formation rates at $z \sim 2$. *Astrophys. J.* **837**, 157 (2017).
139. Jackson, D.C., *et al.* Hot dust and polycyclic aromatic hydrocarbon emission at low metallicity: A *Spitzer* survey of Local Group and other nearby dwarf galaxies. *Astrophys. J.* **646**, 192–204 (2006).
140. Tappe, A., Rho, J. & Reach, W.T. Shock processing of interstellar dust and polycyclic aromatic hydrocarbons in the supernova remnant N132D. *Astrophys. J.* **653**, 267–279 (2006).
141. Seok, J.Y., Koo, B.-C. & Onaka, T. Detection of the 3.3 μm aromatic feature in the supernova remnant N49 with AKARI. *Astrophys. J.* **744**, 160 (2012).
142. Andersen, M., *et al.* Dust processing in supernova remnants: *Spitzer* MIPS spectral energy distribution and *Infrared Spectrograph* observations. *Astrophys. J.* **742**, 7 (2011).
143. Andrews, H., *et al.* PAH emission at the bright locations of PDRs: The grandPAH hypothesis. *Mon. Not. R. Astron. Soc.* **807**, 99 (2015).
144. Kwok, S. & Zhang, Y. Mixed aromatic-aliphatic organic nanoparticles as carriers of unidentified infrared emission features. *Nature* **479**, 80–83 (2011).

145. Salama, F., Joblin, C. & Allamandola, L.J. Neutral and ionized PAHs: Contribution to the interstellar extinction. *Planet. Space Sci.* **43**, 1165–1173 (1995).
146. Clayton, G.C., *et al.* The role of polycyclic aromatic hydrocarbons in ultraviolet extinction. I. Probing small molecular polycyclic aromatic hydrocarbons. *Astrophys. J.* **592**, 947–952 (2003).
147. Buss, R.H., Tielens, A.G.G.M. & Snow, T.P. The mid-infrared spectrum of the carbon star HD38218 and its possible relation to polycyclic aromatic hydrocarbons. *Astrophys. J.* **372**, 281–290 (1991).
148. Speck, A.K. & Barlow, M.J. UIR bands in carbon star spectra. *Ap&SS* **251**, 115–121 (1997).
149. Boersma, C., Hony, S. & Tielens, A.G.G.M. UIR bands in the ISO SWS spectrum of the carbon star TU Tauri. *Astron. Astrophys.* **447**, 213–220 (2006).
150. Sloan, G.C., *et al.* The unusual hydrocarbon emission from the early carbon star HD 100764: The connection between aromatics and aliphatics. *Astrophys. J.* **664**, 1144–1153 (2007).
151. Li, A. & Draine, B.T. Do the infrared emission features need ultraviolet excitation? The polycyclic aromatic hydrocarbon model in UV-poor reflection nebulae. *Astrophys. J.* **572**, 232–237 (2002).
152. Mattioda, A.L., Hudgins, D.M. & Allamandola, L.J. Experimental near-infrared spectroscopy of polycyclic aromatic hydrocarbons between 0.7 and 2.5 μm . *Astrophys. J.* **629**, 1188–1210 (2005).
153. Uchida, K.I., Sellgren, K. & Werner, M.W. Do the infrared emission features need ultraviolet excitation? *Astrophys. J.* **493**, L109–L112 (1998).
154. Jura, M., *et al.* Polycyclic aromatic hydrocarbons orbiting HD 233517, an evolved oxygen-rich red giant. *Astrophys. J.* **637**, L45–L47 (2006).
155. Sandstrom, K.M., *et al.* The *Spitzer* survey of the Small Magellanic Cloud (S³MC): Insights into the life cycle of polycyclic aromatic hydrocarbons. *Astrophys. J.* **715**, 701–723 (2010).
156. Paradis, D., *et al.* Spatial variations of dust abundances across the Large Magellanic Cloud. *Astron. J.* **138**, 196–209 (2009).
157. Lau, R.M., Werner, M.W., Sahai, R. & Ressler, M.E. Evidence from SOFIA imaging of polycyclic aromatic hydrocarbon formation along a recent outflow in NGC 7027. *Astrophys. J.* **833**, 115 (2016).
158. Xie, Y., Ho, L.C., Li, A. & Shangquan, J.Y. The widespread presence of nanometer-size dust grains in the interstellar medium of galaxies. *Astrophys. J.* **867**, 91 (2018).
159. Kwok, S., Volk, K. & Bernath, P. On the origin of infrared plateau features in proto-planetary nebulae. *Astrophys. J.* **554**, L87–L90 (2001).
160. Uchida, K.I., Sellgren, K., Werner, M.W. & Houdashelt, M.L. *Infrared Space Observatory* mid-infrared spectra of reflection nebulae. *Astrophys. J.* **530**, 817–833 (2000).
161. Rapacioli, M., Joblin, C. & Boissel, P. Spectroscopy of polycyclic aromatic hydrocarbons and very small grains in photodissociation regions. *Astron. Astrophys.* **429**, 193–204 (2005).
162. Peeters, E., *et al.* The PAH emission characteristics of the reflection nebula NGC 2023. *Astrophys. J.* **836**, 198 (2017).
163. Xie, Y., Ho, L.C., Li, A. & Shangquan, J.Y. A New technique for measuring polycyclic aromatic hydrocarbon emission in different environments. *Astrophys. J.* **860**, 154 (2018).
164. Cruz-Diaz, G.A., *et al.* PAH products and Pprocessing by different energy sources. *Astrophys. J.* **882**, 44 (2019).
165. An, J.H. & Sellgren, K. Spatial separation of the 3.29 μm emission feature and associated 2 μm continuum in NGC 7023. *Astrophys. J.* **599**, 312–323 (2003).
166. Geballe, T.R., *et al.* Detection of the overtone of the 3.3 μm emission feature in IRAS 21282+5050. *Astrophys. J.* **434**, L15–L18 (1994).
167. Chen, T., Luo, Y. & Li, A. The infrared bands of polycyclic aromatic hydrocarbons in the 1.6–1.7 μm wavelength region. *Astron. Astrophys.* **632**, A71 (2019).
168. Draine, B.T. Can dust explain variations in the D/H ratio? *ASP Conf. Ser.* **348**, 58–69 (2006).
169. Peeters, E., *et al.* Deuterated interstellar polycyclic aromatic hydrocarbons. *Astrophys. J.* **604**, 252–257 (2004).
170. Onaka, T., *et al.* Search for the infrared emission features from deuterated interstellar polycyclic aromatic hydrocarbons. *Astrophys. J.* **780**, 114 (2014).
171. Doney, K.D., Candian, A., Mori, T., Onaka, T. & Tielens, A.G.G.M. Deuterated polycyclic aromatic hydrocarbons: Revisited. *Astron. Astrophys.* **586**, 65–74 (2016).
172. Peeters, E., Tielens, A.G.G.M., Boogert, A.C.A., Hayward, T.L. & Allamandola, L.J. The prominent dust emission feature near 8.9 μm in four HII regions. *Astrophys. J.* **620**, 774–785 (2005).
173. Verstraete, L., *et al.* The aromatic infrared bands as seen by ISO-SWS: Probing the PAH model. *Astron. Astrophys.* **372**, 981–997 (2001).
174. van Diedenhoven, B., *et al.* The profiles of the 3–12 μm polycyclic aromatic hydrocarbon features. *Astron. Astrophys.* **611**, 928–939 (2004).
175. Schütz, O., Meeus, G., Sterzik, M.F. & Peeters, E. Mid-IR observations of circumstellar disks. Part III. A mixed sample of PMS stars and Vega-type objects. *Astron. Astrophys.* **507**, 261–276 (2009).
176. Sloan, G.C., *et al.* Mid-infrared spectra of polycyclic aromatic hydrocarbon emission in Herbig Ae/Be stars. *Astrophys. J.* **632**, 956–963 (2005).
177. Mathis, J.S., Mezger, P.G. & Panagia, N. Interstellar radiation field and dust temperatures in the diffuse interstellar matter and in giant molecular clouds. *Astron. Astrophys.* **128**, 212–229 (1983).
178. Seok, J.Y. & Li, A. Dust and polycyclic aromatic hydrocarbons in the HD 34700 disk. *Astrophys. J.* **809**, 22 (2015).
179. Seok, J.Y. & Li, A. Dust and polycyclic aromatic hydrocarbons in the pre-transitional disk around HD 169142 disk. *Astrophys. J.* **818**, 2 (2016).
180. Berné, O. & Tielens, A.G.G.M. Formation of buckminsterfullerene (C₆₀) in interstellar space. *PNAS* **109**, 401–406 (2012).
181. García-Hernández, D.A., *et al.* The formation of fullerenes: Clues from new C₆₀, C₇₀, and (possible) planar C₂₄ detections in Magellanic Cloud planetary nebulae. *Astrophys. J.* **737**, L30 (2011).
182. Li, Q., Li, A. & Jiang, B.W. How much graphene in space? *Mon. Not. R. Astron. Soc.* **490**, 3875–3881 (2019).
183. Chen, T. & Li, A. Synthesizing carbon nanotubes in space. *Astron. Astrophys.* **631**, A54 (2019).
184. Derenne, S. & Robert, F. Model of molecular structure of the insoluble organic matter isolated from Murchison meteorite. *Meteorit. Planet. Sci.* **45**, 1461–1475 (2010).

Acknowledgements

I dedicate this article to the 60th anniversary of the Department of Astronomy of Beijing Normal University, the 2nd astronomy program in the modern history of China. I thank B.T. Draine, L.C. Ho, M. Karouzos, X.J. Yang and the three anonymous referees for very useful comments and suggestions. I thank L. Armus, P. Beirão, J.G. Ingalls, H. Kaneda, D. Lutz, K. Mattila, D.A. Riechers, B. Siana, O. Vega, M. Yamagishi, and L. Yan for providing the PAH spectra shown in Figs. 1–4. I thank X.Z. Chen, B. Yang and W.B. Zuo for their help during the manuscript preparation. This work is supported in part by NASA grants 80NSSC19K0572 and 80NSSC19K0701.

Competing interests

The author declares no competing financial interests.

Additional information

Correspondence should be addressed to A.L.